UNIVERSIDADE ESTADUAL DE CAMPINAS

Faculdade de Engenharia Elétrica e de Computação

LAÍS ABRANTES VITOI

Analysis of 12 and 24-pulse diode rectifiers operating in aircraft systems with constant and variable frequency

Análise dos retificadores passivos de 12 e 24 pulsos operando em sistemas aeronáuticos com frequência constante e variável

CAMPINAS

2018

LAÍS ABRANTES VITOI

Analysis of 12 and 24-pulse diode rectifiers operating in aircraft systems with constant and variable frequency

Análise dos retificadores passivos de 12 e 24 pulsos operando em sistemas aeronáuticos com frequência constante e variável

Dissertação apresentada à Faculdade de Engenharia Elétrica e de Computação da Universidade Estadual de Campinas como parte dos requisitos exigidos para a obtenção do título de Mestra em Engenharia Elétrica, na área de Energia Elétrica
Dissertation presented to the School of Electrical and Computer Engineering of the University of Campinas in partial fulfillment of the requirements for the degree of Master in Electrical Engineering, in the area of Power Electronics

Orientador: PROF. DR. JOSÉ ANTENOR POMILIO

Este exemplar corresponde à versão final da tese defendida pela aluna LAÍS ABRANTES VITOI, e orientada pelo PROF. DR. JOSÉ ANTENOR POMILIO

CAMPINAS

2018

Agência(s) de fomento e nº(s) de processo(s): CAPES

Ficha catalográfica
Universidade Estadual de Campinas
Biblioteca da Área de Engenharia e Arquitetura
Luciana Pietrosanto Milla - CRB 8/8129

V833a

Vitoi, Laís Abrantes, 1992-
Analysis of 12 and 24-pulse diode rectifiers operating in aircraft systems with constant and variable frequency / Laís Abrantes Vitoi. – Campinas, SP : [s.n.], 2018.

Orientador: José Antenor Pomilio.
Dissertação (mestrado) – Universidade Estadual de Campinas, Faculdade de Engenharia Elétrica e de Computação.

1. Retificadores (Eletrônica). 2. Aeronáutica. 3. Conversores de energia elétrica. I. Pomilio, José Antenor, 1960-. II. Universidade Estadual de Campinas. Faculdade de Engenharia Elétrica e de Computação. III. Título.

Informações para Biblioteca Digital

Título em outro idioma: Análise dos retificadores passivos de 12 e 24 pulsos operando em sistemas aeronáuticos com frequência constante e variável
Palavras-chave em inglês:
Rectifiers (Electronics)
Airplane
Power converters
Área de concentração: Energia Elétrica
Titulação: Mestra em Engenharia Elétrica
Banca examinadora:
José Antenor Pomilio [Orientador]
Flávio Alessandro Serrão Gonçalves
Marcelo Gradella Villalva
Data de defesa: 17-01-2018
Programa de Pós-Graduação: Engenharia Elétrica

COMISSÃO JULGADORA - DISSERTAÇÃO DE MESTRADO

Candidato: Laís Abrantes Vitoi RA: 180552
Data da Defesa: 17 de janeiro de 2018

Título da Tese (inglês): "Analysis of 12 and 24-pulse diode rectifiers operating in aircraft systems with constant and variable frequency".

Título da Tese (português): "Análise dos retificadores passivos de 12 e 24 pulsos operando em sistemas aeronáuticos com frequência constante e variável".

Prof. Dr. José Antenor Pomilio (Presidente, FEEC/UNICAMP)
Prof. Dr. Flávio Alessandro Serrão Gonçalves (UNESP)
Prof. Dr. Marcelo Gradella Villalva (FEEC/UNICAMP)

A ata de defesa, com as respectivas assinaturas dos membros da Comissão Julgadora, encontra-se no processo de vida acadêmica do aluno.

I dedicate this work to all the people that through the knowledge want to grow as person and build a better society.

Acknowledgements

The acknowledgments will be written in Portuguese.

Agradeço primeiramente a Deus, pois tudo o que sou e alcancei devo ao Seu amor infinito.

Aos meus pais, Luiz Henrique e Simone, por serem minha base, fonte de força e determinação. Muito obrigada por me apoiarem, principalmente nos momentos em que a dúvida e o medo estiveram presentes. Ao meu irmão Henrique, pela amizade, carinho e, claro, inúmeras consultorias de inglês. Ao meu noivo Allysson por seu amor, incentivo e apoio diários.

Meus sinceros agradecimentos ao meu orientador, prof. José Antenor Pomilio, por todo o conhecimento transmitido e por dar diretrizes ao trabalho, mas não cercear as individualidades na forma de pesquisar.

Aos meus colegas de laboratório, especialmente Bruno, Diego, Eliabe, Filipe, Hildo, Jefferson, Joel, Nelly e Paloma, pelo aprendizado, troca de experiências, informações e o convívio prazeroso.

À Capes (Coordenação de Aperfeiçoamento de pessoal de nível superior) pelo subsídio financeiro.

With the knowledge we can build a better society. If this work helps at least a person, the effort is already worth.

Abstract

Traditionally, the aeronautical systems operate with fixed frequency (400 Hz), but with the objective of reduce the weight of the airplane and increase the efficiency of the system the aircrafts are becoming more electric (More Electric Aircraft concept). Thus, the airplanes are operating with a variable frequency (360 Hz to 800 Hz) and due to increased power demand, the systems tend to use high voltage dc buses (± 270 V).

In addition, in order to the aircraft operates normally, the systems must comply with aeronautical standards. Two standard aspects will be analyzed in this work: the limits of the source harmonic current and the DC voltage limits.

With the system operating at fixed frequency it is common to use uncontrolled rectifiers at the interface of AC and DC buses. Although with the airplane operating with variable frequency the literature presents few studies with uncontrolled rectifiers.

Thus, this work analyzes uncontrolled rectifiers that provide a bipolar DC voltage (± 270 V) operating with variable frequency. The aim is to verify if these rectifiers can meet the needs of the load and comply with the aeronautical standards. The focus of the work is on the 12-pulse rectifier with two sorts of input filter: L and LC. A mathematical model that includes the harmonic components of the system is developed and allows to analyze the input current and the output voltage. Simulations and a prototype were developed to validate the model. A simplified analysis of the 24-pulse rectifier was also performed using two input filters: L and LC.

Through the analyzes carried out, it is concluded that 12 and 24-pulse uncontrolled rectifiers are not able to meet the aeronautical standards with variable frequency in the considered situations.

Keywords: Bipolar DC buses; More Electric Aircraft; MEA; Variable frequency; 12-pulse rectifier.

Resumo

Tradicionalmente, os sistemas aeronáuticos operam com frequência fixa (400 Hz), mas com o objetivo de reduzir o peso do avião e aumentar a eficiência do sistema, as aeronaves estão se tornando mais elétricas (More Electric Aircraft). Assim, os aviões estão operando com uma frequência variável (360 Hz a 800 Hz) e devido ao aumento da demanda de energia, também tendem a usar barramentos CC de alta tensão (± 270 V).

Além disso, para que a aeronave funcione normalmente, os sistemas devem estar de acordo com as normas aeronáuticas. Dois aspectos das normas serão analisados neste trabalho: os limites da corrente harmônica na fonte e os limites da tensão CC.

Com o sistema que operando em frequência fixa é comum usar retificadores não controlados na interface dos barramentos CA e CC. Entretanto para os sistemas operando em frequência variável a literatura apresenta poucos estudos com retificadores não controlados.

Assim, este trabalho analisa retificadores não controlados que fornecem uma tensão CC bipolar (± 270 V) operando com frequência variável. O objetivo é verificar se esses retificadores podem atender às necessidades da carga e atender aos limites das normas aeronáuticas. O foco do trabalho é no retificador de 12 pulsos com dois tipos de filtro de entrada: L e LC. Um modelo matemático que inclui os componentes harmônicos do sistema é desenvolvido e permite analisar a corrente na fonte e a tensão de saída. Simulações e um protótipo foram desenvolvidos para validar o modelo. Uma análise simplificada do retificador de 24 pulsos também foi realizada usando dois filtros de entrada: L e LC.

Através das análises realizadas, conclui-se que os retificadores não controlados de 12 e 24 pulsos não conseguem atender as normas aeronáuticas quando o sistema opera em frequência variável e nas condições analisadas.

Palavras-chave: Barramento CC bipolar; Frequência variável; More Electric Aircraft; MEA; Retificador de 12 pulsos.

List of Figures

List of Tables

Nomenclature

α_x	Derivative of function $v_{s_{\phi\phi}}$ in the commutations points (θ_x)
Δt	Commutation duration in seconds
Δv_o	Output voltage ripple amplitude - peak to mean
$\Delta\theta$	Commutation duration in radians
$\overline{I_o}$	Output current at each load - average value
$\overline{V_o}$	Average output voltage
$\overline{V_{dc}}$	Voltage at the output of each rectifier - average value
θ_x	Commutation moments in radians
φ_1	Phase angle between $V_{r_{\phi-1}}$ and $I_{r_{\phi-1}}$
$C_{d_{\phi\phi}}$	Damping capacitor (Y connection)
C_{d_ϕ}	Damping capacitor (Δ connection)
$C_{in_{\phi\phi}}$	Capacitance of each input filter - connected between two phases
C_{in_ϕ}	Phase equivalent value of the capacitance of each input filter
C_{out}	Capacitance of the each output filter
f	Supply frequency in hertz
f_c	Cutoff frequency - output filter
h	Harmonic order
i_o	Output current - function representation
i_{d_x}	Current in the diode x of each rectifier - function representation
$i_{L_{in_\phi}}$	Current through L_{in_ϕ} - function representation
$I_{r_{\phi-h}}$	Rms phase current at the input of each rectifier in the harmonic frequency h
$i_{r_{\phi-h}}$	Phase current at the input of each rectifier in the harmonic frequency h - function representation
I_{r_ϕ}	Rms phase current at the input of each rectifier

i_{r_ϕ} Phase current at the input of each rectifier - function representation

I_{s_ϕ} Supply rms phase current

i_{s_ϕ} Supply phase current - function representation

$I_{t_{\phi-h}}$ Rms value of the phase current at the output of each secondary and for the harmonic h

$i_{t_{\phi_{Y\Delta}}}$ Current at the Δ secondary of the transformer - function representation

$i_{t_{\phi_{YY}}}$ Current at the Y secondary of the transformer - function representation

I_{t_ϕ} Rms phase current at the output of each secondary

i_{t_ϕ} Phase current at the output of each secondary - function representation

$L_{in_{\phi_{max}}}$ Maximum value allowed of L_{in_ϕ}

$L_{in_{\phi_{min}}}$ Minimum value allowed of L_{in_ϕ}

L_{in_ϕ} Inductance of each input filter

L_{out} Inductance of the each output filter

N Voltage ratio of the transformer

N_{max} Maximum value allowed for the voltage ratio of the transformer

P_o Output power at one branch of the circuit

$P_{1\phi}$ One phase active power at one branch of the circuit

$P_{3\phi}$ Total active power at one branch of the circuit

$P_{max_{1\phi}}$ Maximum one phase active power at one branch of the circuit

R_1 Resistive part of Z_1

$R_{d_{\phi\phi}}$ Damping resistor (Y connection)

R_{d_ϕ} Damping resistor (Δ connection)

R_o Output resistance of each load

$U_{\phi-h}$ Rms value of $u_{\phi-h}$.

$u_{\phi-h}$ Phase value of the harmonic h of u function defined in equation 2.5

$U_{\phi\phi-h}$ Rms value of $u_{\phi\phi-h}$

$u_{\phi\phi-h}$ Line value of the harmonic h of u function defined in equation 2.5

$u_{\phi\phi}$ u function defined in equation 2.5

v_o Output voltage - function representation

v_{dc} Voltage at the output of each rectifier - function representation

$V_{L_{in_\phi}}$ Voltage over L_{in_ϕ} - rms value

$v_{L_{in_\phi}}$ Voltage across L_{in_ϕ} - function representation

$V_{r_{\phi-h}}$ Rms phase voltage at the input of each rectifier in the harmonic frequency h

$v_{r_{\phi-h}}$ Phase voltage at the input of each rectifier in the harmonic frequency h - function representation

$V_{r_{\phi\phi}}$ Rms line voltage at the input of each rectifier

$v_{r_{\phi\phi}}$ Line voltage at the input of each rectifier - function representation

V_{r_ϕ} Rms phase voltage at the input of each rectifier

v_{r_ϕ} Phase voltage at the input of each rectifier - function representation

$V_{s_{\phi\phi-peak}}$ Peak value of the supply line voltage

$V_{s_{\phi\phi}}$ Supply rms line voltage

$v_{s_{\phi\phi}}$ Supply line voltage - function representation

V_{s_ϕ} Supply rms phase voltage

v_{s_ϕ} Supply phase voltage - function representation

$V_{t_{\phi-h}}$ Rms value of the phase voltage at the output of each secondary and for the harmonic h

$V_{t_{\phi\phi-peak}}$ Peak value of the line voltage at the output of each secondary

$V_{t_{\phi\phi}}$ Rms line voltage at the output of each secondary

$v_{t_{\phi\phi}}$ Line voltage at the output of each secondary - function representation

V_{t_ϕ} Rms phase voltage at the output of each secondary

v_{t_ϕ} Phase voltage at the output of each secondary - function representation

$V_{th_{\phi-1}}$ Thevenin voltage seen by the rectifier at the fundamental frequency - Rms value

w Supply frequency in rad/s

w_r Resonance frequency of each input filer

X_1 Reactive part of Z_1

$X_{th_{\phi-1}}$ Thevenin reactance seen by the rectifier at the fundamental frequency

Z_1 Equivalent impedance seen by the input filter ($Z_1 = V_{r_{\phi-1}}/I_{r_{\phi-1}}$)

Contents

1 Introduction

Traditionally, mechanical, hydraulic, pneumatic and electrical systems comprise the aircraft system (ROSERO *et al.*, 2007) (EMADI; EHSANI, 2000). Although the aeronautical systems are replacing the mechanical, hydraulic and pneumatic systems by electrical systems and becoming more electric (More Electric Aircraft - MEA). Among the benefits of this change it can be highlighted the higher efficiency, safety, reliability and fault tolerance, less maintenance and overall weight of the aircraft (ROSERO *et al.*, 2007; EMADI; EHSANI, 2000; SARLIOGLU; MORRIS, 2015; WHEELER; BOZHKO, 2014).

Following this same concept, eliminating the heavy integrated drive generator (IDG), the variable-speed constant-frequency generation system, that produces the 400 Hz bus, moves to the variable-speed variable-frequency concept producing a 360 to 800 Hz bus (SARLIOGLU; MORRIS, 2015). Thus the loads must be prepared to operate in a system of variable frequency.

The energy distribution system in the aircraft includes different buses: 28 V DC, 270 V DC, 115 V AC (Figure 1) (WHEELER; BOZHKO, 2014; FADIL A.E., 2013) . Due to the electric power demand increase, a high-voltage (270 V DC) bus has been created and, more recently, in a bipolar version (± 270 V - 540 V) (NYA *et al.*, 2012). With this increase in voltage, for the same power, the current is lower, consequently the weight of the cables is reduced, which is important for aeronautical systems (WHEELER; BOZHKO, 2014). With the bipolar bus it is possible to connect simultaneously loads of 270 V and 540 V. There is also a tendency to raise the AC voltage level from 115 V to 230 V, but this will not be analyzed in this work.

1.1 Standards and Operation Condition

Normalization is the establishment of specifications that aim to maximize compatibility, safety and quality in a given system or product. In aviation systems, it is expected that, after the connection of all elements, the aircraft operates as desired and, mainly, with safety. Among the main aviation standards are highlighted MIL-STD-704F (STATES, 2008) and RTCA DO-160F (STATES, 2007) which provide, respectively, the aircraft electric power characteristics and the environmental conditions and test procedures for airborne equipment.

Among the features analyzed on the RTCA DO-160F it is included how the load influences on the aircraft electrical power system. One of the requirements that shall

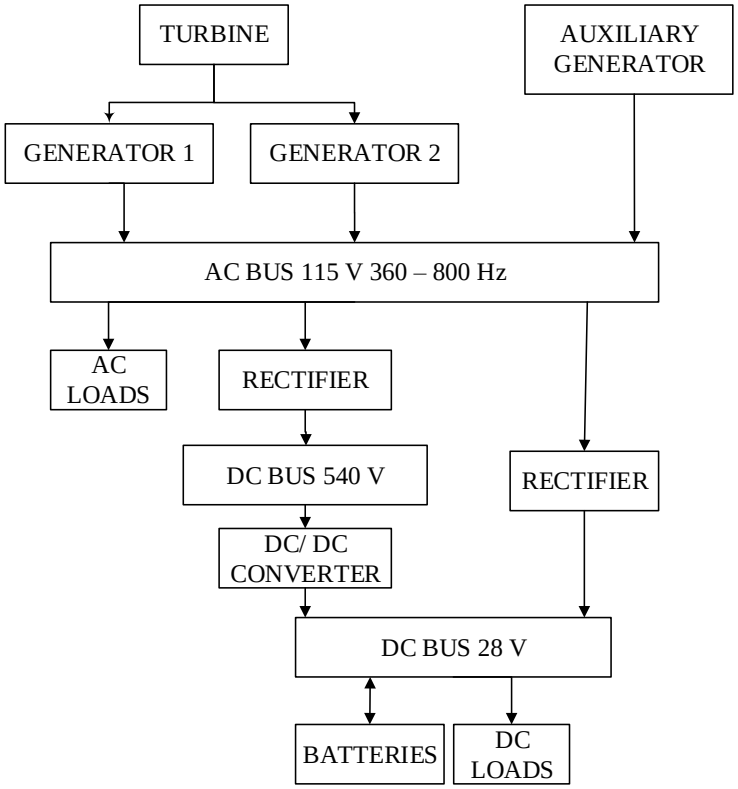

Figure 1 – Typical modern airplane electric network.

be meet is the maximum harmonic currents demanded from the source. The standard is too restrictive, especially with respect to low order harmonics. For the 11^{th} and 13^{th} are acceptable 10% and 8% of the fundamental respectively, while for the 3^{rd}, 5^{th}, and 7^{th} the limit is 2% of the fundamental component at the maximum demand. In a variable frequency system the fundamental value is moving. The system should ensure that the fundamental is accurately measured and the harmonics are calculated based on this measurement. The limits for Balanced Three-Phase Electrical Equipment are shown in Table 1.

The MIL-STD-704F establishes that the AC three phase voltage of the power source shall be a sine wave with a nominal voltage of 115 V and a nominal frequency of 400 Hz, although, it is allowed the use of variable frequency (360 - 800 Hz). The AC system is regulated using some features that are defined for normal and abnormal conditions. The limits for the AC voltage and frequency in the steady state of the normal condition are shown in Table 2. For the DC bus the nominal voltage can be 28 V or 270 V volts and normal and abnormal operating conditions are also defined. The 28 V bus is the traditional DC bus, but in airplanes with higher power demand the 270 V DC bus is also used. For the 270 V system, among other parameters, are highlighted the limits of nominal voltage

Table 1 – Current harmonic limits for balanced three-phase electrical equipment.

Harmonic order	Limits
3^{rd}, 5^{th}, 7^{th}	$I_3 = I_5 = I_7 = 0.02I_1$
Odd triplen harmonics (h = 9, 15, 21, ..., 39)	$I_h = 0.1I_1/h$
11^{th}	$I_{11} = 0.1I_1$
13^{th}	$I_{13} = 0.08I_1$
Odd non triplen harmonics 17, 19	$I_{17} = I_{19} = 0.04I_1$
Odd non triplen harmonics 23, 25	$I_{23} = I_{25} = 0.03I_1$
Odd non triplen harmonics 29, 31, 35, 37	$I_h = 0.3I_1/h$
Even harmonics 2 and 4	$I_h = 0.01I_1/h$
Even harmonics > 4 (h = 6, 8, 10, ..., 40)	$I_h = 0.0025I_1$
I_1 = maximum fundamental current of the equipment that is measured during the maximum steady-state power demand operating mode condition, at a single test frequency h = order of harmonic I_h = maximum harmonic current of order h obtained for all normal steady state modes of operation.	

and ripple amplitude in the steady state of the normal operation (Table 2). The present work deals with 540 V (± 270 V) DC systems. Nonetheless, there are no published aircraft standards for the power quality for this voltage level thus, the analysis and results are compared with the limits of MIL-STD-704F to 270 V.

Table 2 – AC and DC normal operation characteristics.

AC BUS	
Frequency (f)	360 to 800 Hz
Steady state voltage – phase voltage (V_{s_ϕ})	108.0 to 118.0 Volts, RMS
270 V DC BUS	
Steady state voltage ($\overline{V_o}$)	250 to 280 V
Ripple amplitude - peak to mean (Δv_o)	6.0 Volts maximum

This work deals with the rectifier module (Figure 1). The rectifier seen by the DC bus and loads is taken as a source, therefore, it should comply with the sources standard (MIL-STD-704F). Although, seen by the AC bus, the rectifier is a load, thus it should also obey the limits and requirements imposed for the loads (RTCA DO-160F).

1.2 Aim and structure of the text

Most articles dealing with variable frequency aeronautical systems use controlled rectifiers and do not analyze the possibility of using uncontrolled rectifiers. Therefore, this work aims to develop a systematic analysis of uncontrolled rectifiers that can provide a bipolar output voltage and that meet aeronautical standards.

This thesis analyzes rectifiers that create a bipolar DC voltage, considering the system operates with constant frequency (400 Hz) and variable frequency (360-800 Hz), with the specifications given in Table 2 and complying with the current harmonic limits established by the standard RTCA DO-160F (Table 1). The analyzes will be done for an aeronautical system of 50 kW (25 kW for each rectifier), which is compatible with medium size aircrafts.

This work is divided in two parts, the first one analyses the uncontrolled 12-pulse rectifier operating with fixed and variable frequencies. In this part is considered two types of input filter: L and LC. For each case is developed a mathematical model, a PLECS simulation and a prototype is assembled to validate the results.

In the second part the uncontrolled 24-pulse rectifier is analyzed. In this case the analyzes are less deep, but it gives a good insight to the reader about the subject.

1.3 Introduction 12-pulse rectifier

The rectifier behavior must, among other properties, comply with the specifications of RTCA DO-160F for the current harmonics and with MIL-1000-704F specifications with regard to the AC and DC buses. The usual solution for fixed frequency networks is the use of the TRU (Transformer Rectifier Unit) or ATRU (Autotransformer Rectifier Unit). The harmonic restrictions imply the use of, at least, a 12-pulse topology, as shown in Figure 2 (MONROY *et al.*, 2012). This topology appears as a good solution due to its low harmonic, simple structure, high reliability, strong overload capacity, does not require control electronics and its configuration allows an implementation of symmetric buses without the need of an additional circuit. However, it is relatively heavy and presents low power density due to the transformer (GONG *et al.*, 2003; KARIMI; MONG, 2002; JIANG *et al.*, 2012; MINO *et al.*, 2005; SILVA *et al.*, 2014).

This topology consists of two six-pulse rectifiers, one connected through a Y-Δ transformer and the other through a Y-Y transformer, resulting AC currents with 30°phase shift, producing a 12-pulse rectification and a primary current with 6 levels (Figure 3). If the currents in both 6-pulse rectifiers are equal, an effective cancellation of the 5^{th} and 7^{th} harmonics occurs and the input current harmonics appears at multiples of the pulse number, i.e., show harmonic currents only at h=11,13,23,25... The output of the

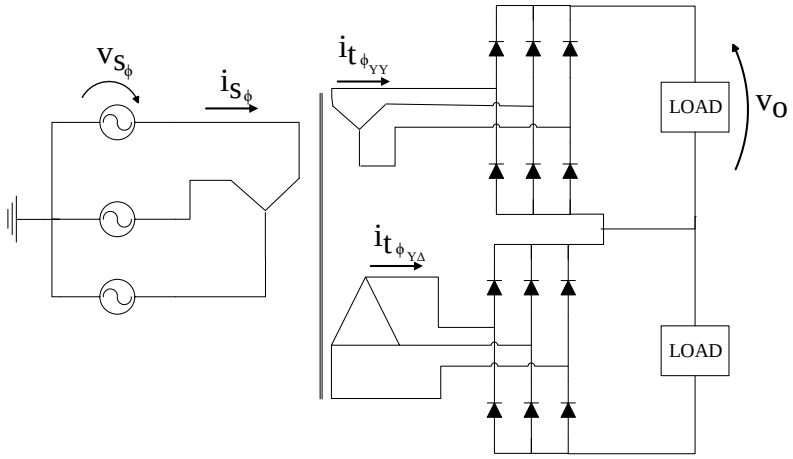

Figure 2 – Topology of a passive three-phase 12-pulse rectifier.

rectifiers are connected in series to generate the bipolar DC buses (± 270 V). Rectifiers connected in parallel are used when it is desired to produce a simple 270 V DC bus.

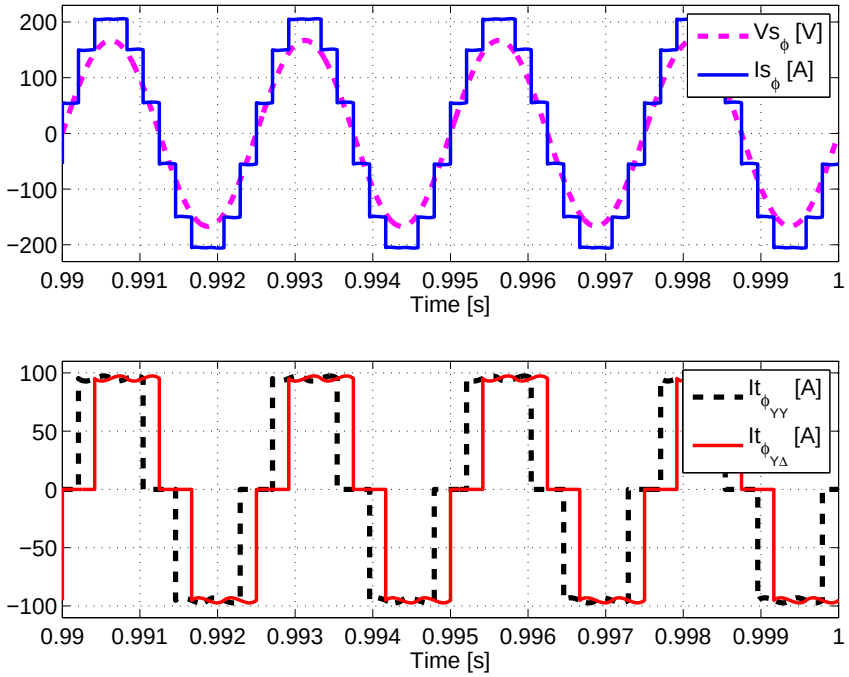

Figure 3 – Current and voltage at the primary of the transformer (top) and currents at the secondaries of the transformer (below).

The most relevant articles founded about 12-pulse rectifiers applied to aeronautical systems are from a Switzerland research group (GONG *et al.*, 2003; MINO *et al.*, 2005; GONG *et al.*, 2005; GONG *et al.*, 2004). The papers consider the variable frequency system and work with 5 kW and 10 kW. In the papers (GONG *et al.*, 2003; GONG *et al.*, 2004) and (GONG *et al.*, 2005) the circuit shown is Figure 4, the output of the 6-pulse

rectifiers are connected in parallel, providing only one level of DC voltage and utilizes an input inductor to limit the harmonic currents. In (GONG *et al.*, 2005) the interferences and limitations in the output voltage and power, and the mains current quality are analyzed in some details.

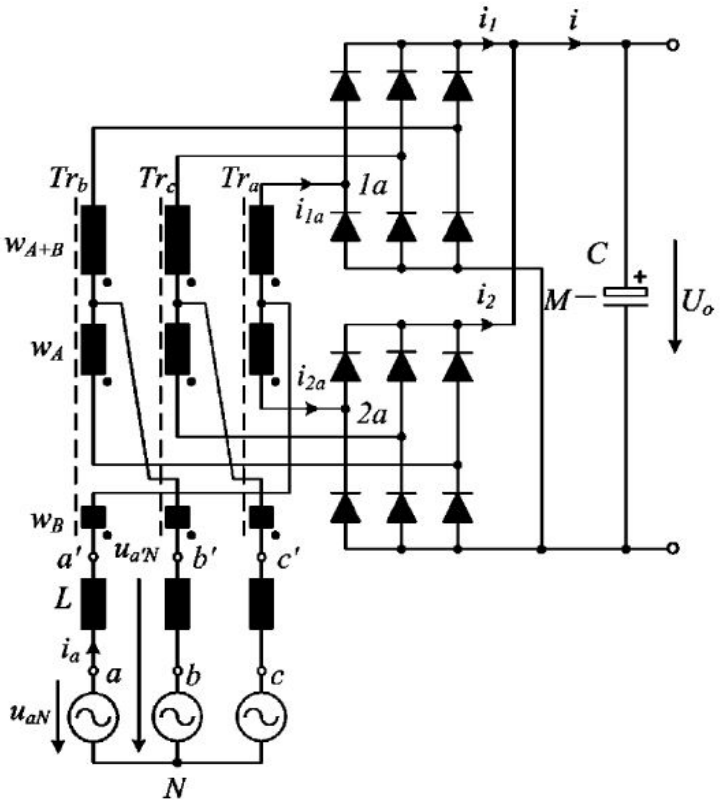

Figure 4 – 12-pulse rectifier studied by (GONG *et al.*, 2003; MINO *et al.*, 2005; GONG *et al.*, 2005; GONG *et al.*, 2004).

The paper (CROSS *et al.*, 2009) does a modeling for the 12-pulse rectifier with a L input filter and the output of the rectifiers connected in parallel. The paper presents the model and compares it with results of a prototype but does not analyze whether the output voltage and source harmonic current meet the limits of aeronautical standards.

In addition, from this present work two papers have been originated until the present moment. The (VITOI *et al.*, 2017a) and (VITOI *et al.*, 2017b) deal with the 12-pulse rectifier applied to aeronautical systems with fixed and variable frequency, respectively.

The total power considered in this work is 50 kW (25 kW for each rectifier) which is compatible with medium size aircrafts. The loads are modeled as constant power once the DC loads are mostly electronic and the constant power model best approximates its behavior. The results are shown only for one of the rectifiers, once it is considered that the loads are balanced and the results in both rectifiers are the same. During the

text the subscripts ϕ and $\phi\phi$ appear, they indicate whether it is the phase-neutral or the equivalent phase-phase value of each variable, respectively.

2 Model and design

2.1 Design of the output filter

To ensure that the output voltage ripple complies with the standards, it is necessary to use a DC filter. A simple solution is a passive filter. It was chosen a second-order LC filter (Figure 5) once it offers a good filtering with the possibility of smaller components.

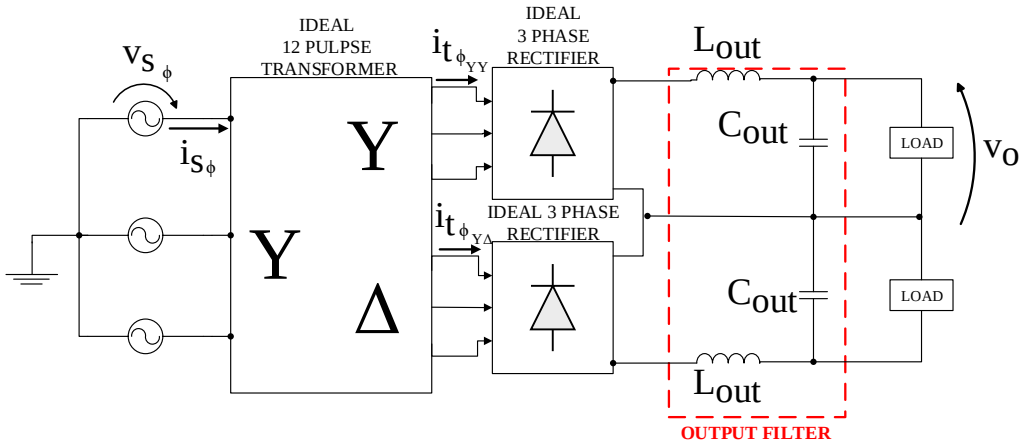

Figure 5 – Schematic of 12-pulse rectifier with LC DC filter.

The LC filter used on the DC side of the rectifier must take into account firstly the filter requirement, considering the AC frequency and the rectifier behavior. The voltage ripple at the output of the rectifier has a frequency of six times the AC frequency. The peak to peak voltage ripple to be applied to the filter is approximately 36 V (V_{s_ϕ} = 115 V), 13% of the peak value of the AC line voltage. According to the standard, the maximum ripple amplitude is 6 V. In order to operate with an adequate margin regarding such limits, as well to allow a proper reduction of ripple in case of imbalances (provided in the standard), it is possible to determine the cutoff frequency of the filter, which was stipulated around 500 Hz. Thus, it has been known product LC of the output filter.

Following, it is necessary to determine the inductance taking into account the current ripple, which, in turn, is related to the capacitor capacity of conduction. A higher reliability of the capacitor depends on its temperature, which is determined by the current value and the equivalent series resistance (R_{se}). The current value is limited by the inductor and the capacitor (or association of capacitors) must be determined in order to reduce R_{se}, limiting the losses and device heating.

Approaching the voltage ripple by a sinusoid and stipulating a current ripple of 1.5 A, an inductance of approximately 500 µH is obtained, which leads to a capacitance of 200 µF. The capacitor must be selected to allow such current without producing excessive raise in temperature. The Table 3 shows the circuit values for the DC filter design. The parameters of the filter were designed for the worst ripple situation to ensure that the circuit comply with the ripple limits in all operation conditions.

Table 3 – Design the LC DC filter.

Variable	Symbol	Value
Maximum DC ripple allowed	Δv_o	6 V
Power in each rectifier	$P_{3\phi}$	25 kW
Voltage ratio	N	1
Cutoff frequency - output filter	f_c	500 Hz
Output inductor	L_{out}	500 µH
Output capacitor	C_{out}	200 µF

The Figure 6 shows the load voltage and Figure 7 shows the voltage and current at the source, respectively. The current source harmonic content is given in Figure 8 and Table 4. As can be seen, with the DC filter, the output voltage ripple limit is respected, although the harmonic content of the current source is beyond the acceptable values for the higher harmonics, thereby, it is necessary to reduce some harmonics, what will be done with the use of an AC filter.

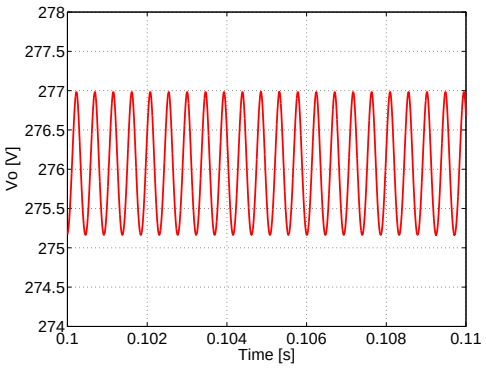

Figure 6 – Output voltage (red) with an LC DC filter - $V_{s_\phi} = 118$ V and $f = 360$ Hz.

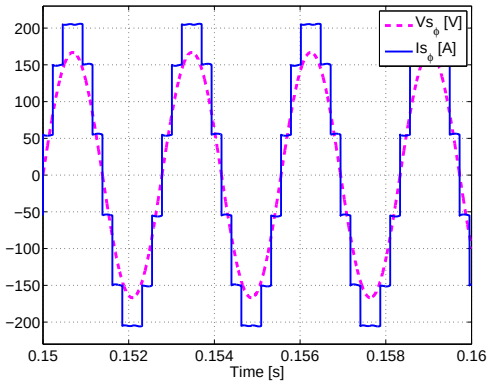

Figure 7 – Input voltage (magenta) and current (blue) with an LC DC filter - $V_{s_\phi} = 118$ V and $f = 360$ Hz.

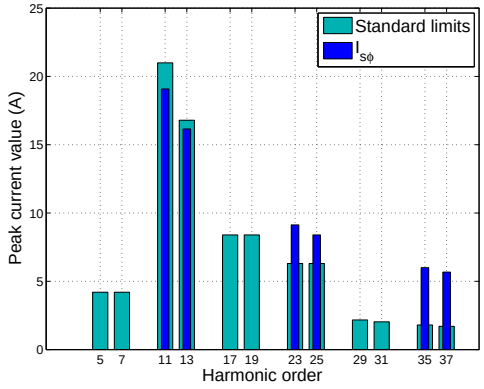

Figure 8 – Harmonic content of the input current with LC DC filter - $V_{s_\phi} = 118$ V and $f = 360$ Hz.

Table 4 – Numeric values of the Figure 8 - Harmonic content of the input current with LC DC filter - $V_{s_\phi} = 118$ V and $f = 360$ Hz.

Harmonic order	I_{s_ϕ} - peak values (A)
1	209.9
11	19.1
13	16.1
23	9.1
25	8.4
35	6
37	5.7

2.2 First order input L filter

As can be seen, the output filter solves the output voltage ripple problem, but the harmonics of the input current are above the standard limits. Thus, it is required to use an input filter in order to minimize the input current harmonics. Figure 9 shows the circuit with the L input filter (L_{in_ϕ}), the simplest solution to limit the AC current harmonics. The aim is to meet the aeronautical standards in regard to both aspects: the output voltage and the harmonics of the input current. For the analysis, all the elements are considered ideal. The inductance of the source and the transformer are included in the L_{in_ϕ} value.

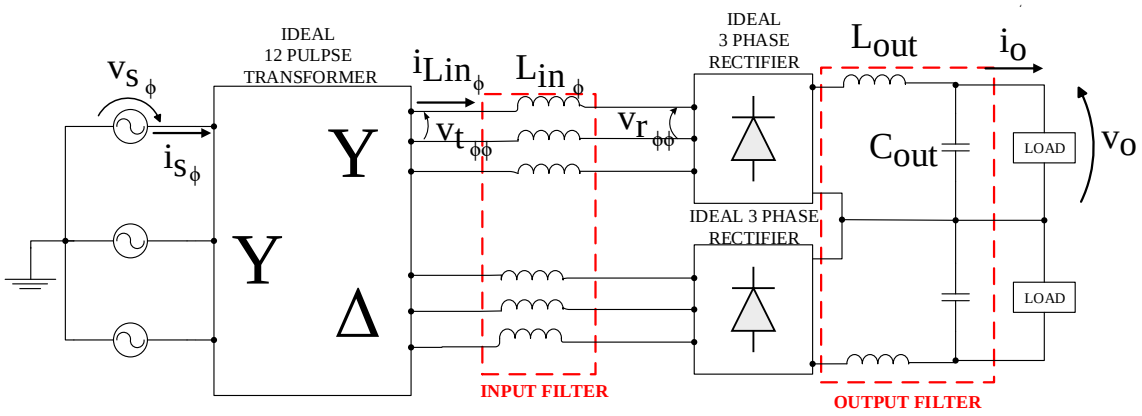

Figure 9 – Circuit using the input L filter.

2.2.1 Mathematical modeling

The input inductor can limit the AC harmonic currents. On the other hand, the presence of such input inductor produces the so called commutation phenomenon, in which two diodes of the same half bridge conduct simultaneously. This behavior causes a voltage notch in the input voltage of the rectifier ($v_{r_{\phi\phi}}$) (Figure 10), reducing the DC voltage (RASHID, 1999).

Considering the output current ripple is so small that the respective voltage drop in the input inductor can be neglected, the rectifier operates in the continuous mode and the input current varies approximately linearly during the commutation interval, it is possible to determine the resulting output average DC voltage ($\overline{V_o}$) including the commutation effect by the equation (2.1) (RASHID, 1999). Where V_{t_ϕ} is the RMS phase voltage at the output of the transformer.

$$\overline{V_o} = \frac{3\sqrt{6}}{\pi} V_{t_\phi} - 6 f L_{in_\phi} \overline{I_o} \tag{2.1}$$

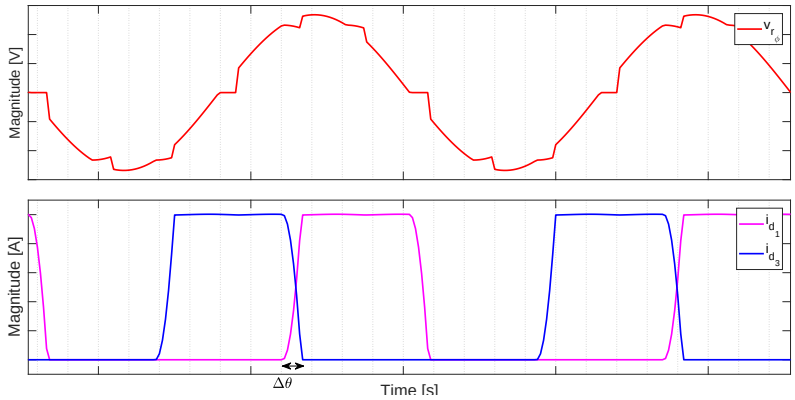

Figure 10 – Notch effect: rectifier input voltage (above) and current in diodes D1 and D3 (below).

Modeling the load as a constant power device and considering the voltage ratio of the transformer (N), it is found (2.2). Thus, it is possible to establish the maximum value of the input inductor ($L_{in_{\phi max}}$) to produce the minimum allowed output voltage (250 V) with the worst operating condition for each case.

$$\overline{V_o}P_{3\phi} - \frac{3\sqrt{6}}{\pi}V_{s_\phi}NP_{3\phi} + 6fL_{in_\phi}\overline{V_o} = 0 \tag{2.2}$$

To calculate the minimum inductance value ($L_{in_{\phi min}}$) that satisfies the harmonic current limits it is analyzed the rectifier input voltage (Figure 10). Considering that in the commutation intervals (that start at $\theta_x = 0$, $\pi/3$, $2\pi/3$, π, $4\pi/3$ and $5\pi/3$ rad) the rectifier input voltage remains approximately constant, $v_{r_{\phi\phi}}$ can be written by (2.3) or (2.4).

$$v_{r_{\phi\phi}}(\theta) = v_{t_{\phi\phi}}(\theta) - u_{\phi\phi}(\theta) \tag{2.3}$$

$$v_{r_{\phi\phi}}(\theta) = v_{s_{\phi\phi}}(\theta)N - u_{\phi\phi}(\theta) \tag{2.4}$$

Where $u_{\phi\phi}$ is defined as (2.5). The Figure 11 shows the graph of the $u_{\phi\phi}$ function.

$$u_{\phi\phi}(\theta) = \begin{cases} N(v_{s_{\phi\phi}}(\theta) - v_{s_{\phi\phi}}(\theta_x)), & \text{if } \theta_x \leq \theta \leq \theta_x + \Delta\theta \\ 0, & \text{otherwise} \end{cases} \tag{2.5}$$

Where $\Delta\theta$ is the commutation duration in radians (Figure 10).

As $v_{s_{\phi\phi}}$ is a pure sine wave, the harmonic content of $v_{r_{\phi\phi}}$ is entirely present in the function $u_{\phi\phi}$. To simplify the calculation, the sinusoidal voltage is approximated by a

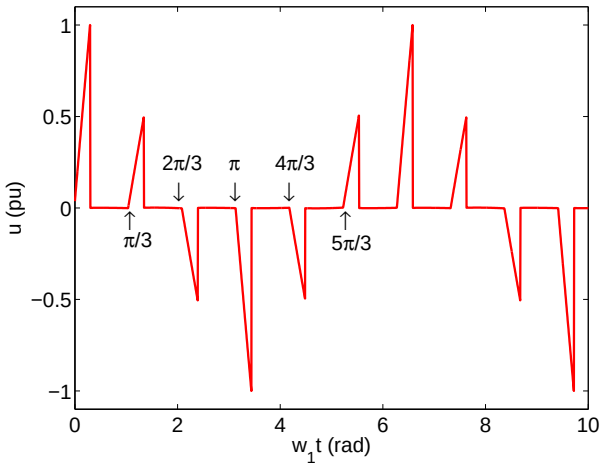

Figure 11 – Graph of $u_{\phi\phi}$ function.

straight line in each commutation point (θ_x) (first order Taylor approximation). Therefore, $v_{s_{\phi\phi}}$ can be written as (2.6).

$$v_{s_{\phi\phi}}(\theta) = \alpha_x(\theta - \theta_x) + v_{s_{\phi\phi}}(\theta_x) \tag{2.6}$$

Where α_x is the derivative of function $v_{s_{\phi\phi}}$ in the commutations points (θ_x) (Table 5).

Table 5 – Derivative of function $v_{s_{\phi\phi}}$ in θ_x.

θ_x (rad)	α_x (rad)
0	$V_{r_{\phi\phi-peak}}$
$\pi/3$	$0.5V_{r_{\phi\phi-peak}}$
$2\pi/3$	$-0.5V_{r_{\phi\phi-peak}}$
π	$-V_{r_{\phi\phi-peak}}$
$4\pi/3$	$-0.5V_{r_{\phi\phi-peak}}$
$5\pi/3$	$0.5V_{r_{\phi\phi-peak}}$

Substituting (2.6) into (2.5) it can be found a simpler equation for $u_{\phi\phi}$.

$$u_{\phi\phi}(\theta) = \begin{cases} N\alpha_x(\theta - \theta_x), & \text{if } \theta_x \leq \theta \leq \theta_x + \Delta\theta \\ 0, & \text{otherwise} \end{cases} \tag{2.7}$$

The Equation (2.8) is the Fourier series of $u_{\phi\phi}$. The Equations (2.9) and (2.10) show the Fourier coefficients of the $u_{\phi\phi}$ function.

$$u_{\phi\phi}(\theta) = A_0 + \sum_{n=1}^{\infty} A_n \cos(n\theta) + \sum_{n=1}^{\infty} B_n \sin(n\theta) \tag{2.8}$$

$$A_n = \frac{1}{\pi}\sum_{\theta_x}\left[\frac{\alpha_x \sin(n\theta)}{n}(\theta-\theta_x)+\frac{\alpha_x \cos(n\theta)}{n^2}\right]\Bigg|_{\theta_x}^{\theta_x+\Delta\theta} \tag{2.9}$$

$$B_n = \frac{1}{\pi}\sum_{\theta_x}\left[\frac{\alpha_x \cos(n\theta)}{n}(\theta_x-\theta)+\frac{\alpha_x \sin(n\theta)}{n^2}\right]\Bigg|_{\theta_x}^{\theta_x+\Delta\theta} \tag{2.10}$$

The coefficients are a function of $\Delta\theta$. To calculate the values some considerations are made:

- The input current ($i_{L_{in_\phi}}$) varies linearly during the commutation interval.

$$v_{L_{in_\phi}} = L_{in_\phi}\frac{\partial i_{L_{in_\phi}}}{\partial t} = L_{in_\phi}\frac{\Delta i_{L_{in_\phi}}}{\Delta t} \tag{2.11}$$

$$V_{L_{in_\phi}} = L_{in_\phi}\frac{\overline{I_o}}{\Delta t} \tag{2.12}$$

- The sinusoidal voltage source is approximated by a straight. As the commutation durations are the same for all θ_x, the calculation is done at $\theta_x = 0$ rad.

$$v_{s_{\phi\phi}}(\theta) = V_{s_{\phi\phi-peak}}\theta \tag{2.13}$$

$$v_{s_{\phi\phi}}(t) = V_{s_{\phi\phi-peak}}wt = \frac{V_{t_{\phi\phi-peak}}wt}{N} \tag{2.14}$$

- The voltages across the inductors involved in the commutation are equal, approximately constant, and assume the instantaneous value of $v_{t_{\phi\phi}}/2$ at half of the commutation interval. Using (2.13) it is found (2.15).

$$V_{L_{in_\phi}} = \frac{v_{t_{\phi\phi}}(\Delta t/2)}{2} = \frac{V_{t_{\phi\phi-peak}}w\Delta t}{4} \tag{2.15}$$

Substituting (2.15) into (2.11), the duration of the commutation is:

$$\Delta t = \sqrt{\frac{4L_{in_\phi}\overline{I_o}}{V_{t_{\phi\phi-peak}}w}} \tag{2.16}$$

$$\Delta\theta = w_1\sqrt{\frac{4L_{in_\phi}\overline{I_o}}{V_{t_{\phi\phi-peak}}w}} \tag{2.17}$$

Thereby, using (2.9), (2.10) and (2.17) it is possible to find the harmonic components of $u_{\phi\phi}$ (Equation (2.8)).

Analyzing the phase diagram for each harmonic (Figure 12), the inductor voltage drop is directly determined by the $u_{\phi-h}$ function. $U_{\phi-h}$ and $U_{\phi\phi-h}$ are the RMS values of $u_{\phi-h}$ and $u_{\phi\phi-h}$ respectively. Thus, the harmonic currents are defined by 2.20.

$$V_{L_{in_{\phi-h}}} = V_{t_{\phi-h}} - (V_{t_{\phi-h}} - U_{\phi-h}) \tag{2.18}$$

$$V_{L_{in_{\phi-h}}} = U_{\phi-h} = \frac{U_{\phi\phi-h}}{\sqrt{3}} = hwL_{in_\phi} I_{t_{\phi-h}} \tag{2.19}$$

$$I_{t_{\phi-h}} = \frac{U_{\phi\phi-h}}{\sqrt{3}hwL_{in_\phi}} \tag{2.20}$$

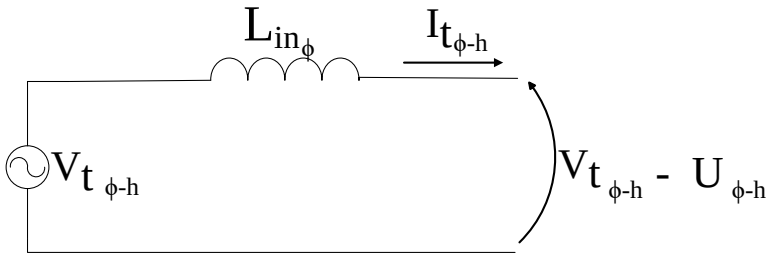

Figure 12 – Phase diagram for each harmonic (h).

Considering the load is balanced, the input current in the 12-pulse transformer is zero for even harmonics and for the multiple of three. For odd components it is twice of the value at the secondary windings (equation 2.20). Therefore, it is possible to find the minimum value of L_{in_ϕ} that complies with the standards limits (Table 1) using a computational software (e.g. Matlab) to solve Equation 2.20.

It's possible to use a different transformer voltage ratio. Although, N has a maximum value to comply with the output voltage ($\overline{V_o}$) limit (280 V). It is possible to establish this value using equation (2.1) and adopting the worst conditions: $V_{s_\phi} = 118\,\text{V}$, $L_{in_\phi} = 0\,\text{H}$ and $\overline{V_o}$ =280 V. Thus, it is found equation (2.21) and the maximum value is $N_{max} = 1.0144$.

$$\overline{V_o} = \frac{3\sqrt{6}}{\pi} V_{s_\phi} N \tag{2.21}$$

2.2.2 Analysis of the circuit operating with fixed frequency (400 Hz)

To validate the mathematical model developed it was implemented in the software Matlab and compared with the circuit simulation at the software Plecs.

2.2.2.1 Analysis of the model at Matlab with fixed frequency

The mathematical model allows to calculate the maximum and minimum values that L_{in_ϕ} can assume. As the operation frequency is fixed, the only variable that influences $L_{in_{\phi_{min}}}$ and $L_{in_{\phi_{max}}}$ is the voltage source (V_{s_ϕ}).

As previously explained, L_{in_ϕ} should limit the harmonic input currents to meet the standards, thus the value of $L_{in_{\phi_{min}}}$ depends on the harmonic input currents and the worst condition for this case is with the maximum voltage source ($V_{s_\phi} = 118\,\text{V}$). Although, the inductor causes a drop in the output voltage, thus there is a maximum value that L_{in_ϕ} can assume in order to $\overline{V_o}$ be above the limit (250 V) with the worst operation condition for this case ($V_{s_\phi} = 108\,\text{V}$). Table 6 summarizes how this analysis is done.

Table 6 – Conditions for the calculation of $L_{in_{\phi_{min}}}$ and $L_{in_{\phi_{max}}}$ with fixed frequency.

Variable	Symbol	Value	
		$L_{in_{\phi_{min}}}$	$L_{in_{\phi_{max}}}$
Supply rms phase voltage	V_{s_ϕ}	118 V	108 V
Limiting condition	-	Harmonics of I_s	$V_o = 250\,\text{V}$
Supply frequency	f	400 Hz	

Initially it was used unitary voltage ratio ($N = 1$). For the calculation of $L_{in_{\phi_{min}}}$ and $L_{in_{\phi_{max}}}$ the equations (2.2) and (2.20) were used with the data from Table 6. The Matlab fzero function was used and the graph of the maximum and minimum values of L_{in_ϕ} was plotted as a function of the output power ($P_{3\phi}$) (Figure 13). As can be seen, for the entire power range, the value of $L_{in_{\phi_{min}}}$ is greater than $L_{in_{\phi_{max}}}$, which means that it is not possible to meet the two conditions.

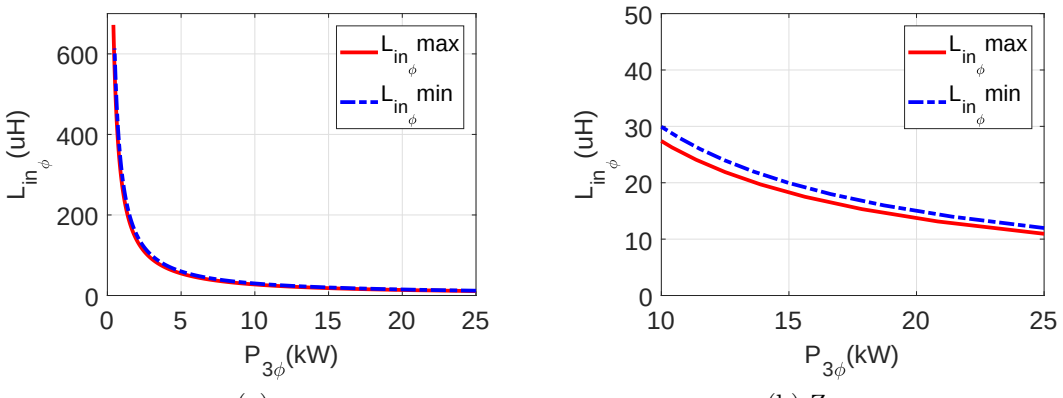

(a) (b) Zoom

Figure 13 – Maximum and minimum values of the input inductor for N=1 and $f = 400\,\text{Hz}$.

A possible solution is to change the voltage ratio of the transformer. As shown in the mathematical modeling, the maximum value that N can assume is 1.0144 (Equation

(2.21)). Using this value and performing the same procedure, there is the new graph of L_{in_ϕ} (Figure 14).

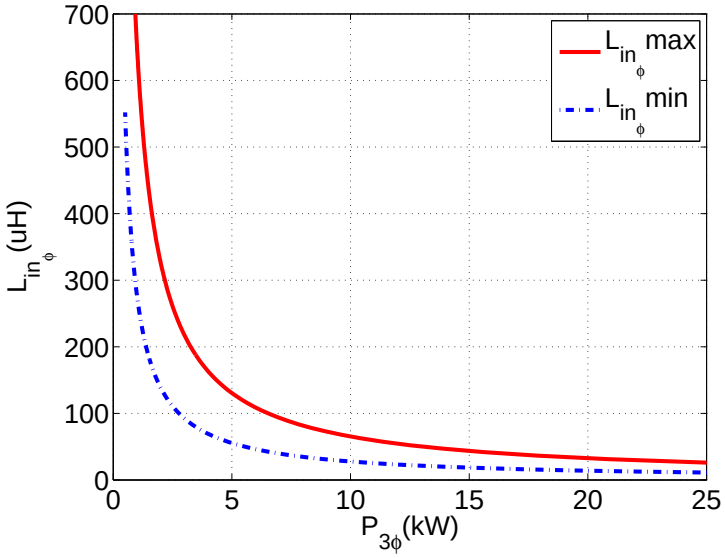

Figure 14 – Maximum and minimum value of the input inductor with N=1.0144 and f = 400 Hz.

As can be seen, with $N = 1.0144$ it is possible to find an inductance value that satisfies both conditions. For the rated power (25 kW) this value should be between 11.13 µH and 26.1 µH.

2.2.2.2 Circuit simulation with PLECS for fixed frequency

To validate the mathematical model, the circuit was simulated in the software PLECS with $L_{in_{\phi_{min}}}$ (11.13 µH) and $L_{in_{\phi_{max}}}$ (26.1 µH). The other circuit parameters are presented in Table 7 and Figure 15 shows the PLECS diagram.

Table 7 – Plecs simulation parameters with fixed frequency - L filter.

Variable	Symbol	Value	
		$L_{in_\phi=}$ 11.13 µH	$L_{in_\phi=}$ 26.1 µF
Supply rms phase voltage	V_{s_ϕ}	118 V	108 V
Supply frequency	f	400 Hz	
Output filter inductor	L_{out}	500 µH	
Output filter capacitor	C_{out}	200 µF	
Power in each rectifier	$P_{3\phi}$	25 kW	
Voltage ratio	N	1.0144	

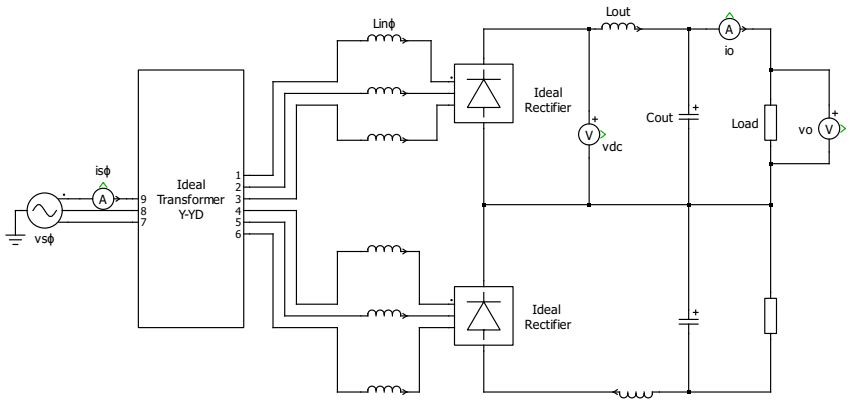

Figure 15 – Circuit diagram at software PLECS.

The Figure 16 shows the output voltage with $L_{in_{\phi max}} = 26.1\,\mu\text{H}$. The average output voltage in the simulation is 249.9 V, which is really close to expected according to the mathematical model ($\overline{V_o} = 250\,\text{V}$).

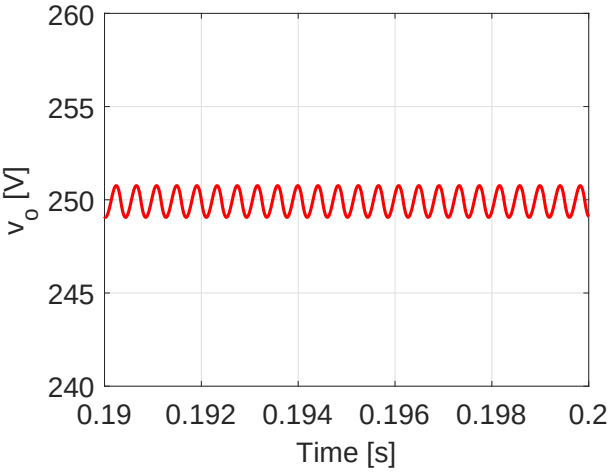

Figure 16 – Simulation - output voltage with L filter - $f = 400\,\text{Hz}$ and $V_{s_\phi} = 108\,\text{V}$.

With the minimum inductor (11.13 µH) it was analyzed the harmonic content of the source current. The Figure 17 shows the waveform of the input current and Table 8 shows the comparison between the simulated and calculated values. As calculated in the previous section, these values meet the standards. As can be seen, their values are very close, the small differences are due to the mathematical model assumes a constant output current while in the simulation the output current has a small ripple.

This section showed that the mathematical model is in agreement with the simulation results and that there is a feasible numerical value for L_{in_ϕ}. Nonetheless, this value is too small to be used in a real situation once the model is not considering the losses, the inductances of transformers, wires and generator and voltage drops on diodes (GONG *et al.*, 2003; MINO *et al.*, 2005; GONG *et al.*, 2005; BAGHRAMIAN *et al.*, 2011; CHIVITE-ZABALZA; FORSYTH, 2005; CROSS *et al.*, 2009).

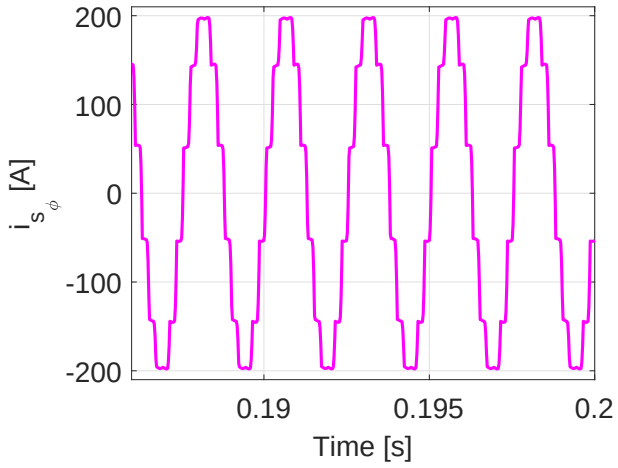

Figure 17 – Simulation - input current with L filter - $f = 400\,\text{Hz}$ and $V_{s_\phi} = 118\,\text{V}$.

Table 8 – Harmonic content of input current - comparison between the simulated and calculated values - $f = 400\,\text{Hz}$, $V_{s_\phi} = 118\,\text{V}$ and $L_{in_{\phi_{min}}} = 11.13\,\mu\text{H}$

Harmonic order	Peak value - calculation (A)	Peak value - simulation (A)
11	16.074	16.249
13	12.975	12.667
23	5.094	5.115
25	4.242	4.269
35	1.694	1.718
37	1.442	1.476

2.2.3 Analysis of the circuit operating with variable frequency (360 - 800 Hz)

Similar to the previous analysis, it is compared the mathematical model implemented in the software Matlab with the circuit simulation at PLECS.

2.2.3.1 Analysis of the model at Matlab with variable frequency

When the system operates at fixed frequency, only the voltage source determines the worst operating condition. With the system operating at variable frequency the worst operating condition is given by both, the source voltage and the frequency. Table 9 summarizes the conditions to calculate the values of $L_{in_{\phi_{min}}}$ and $L_{in_{\phi_{max}}}$.

For $N = 1$, the calculation of $L_{in_{\phi_{max}}}$ uses equation (2.2). And for $L_{in_{\phi_{min}}}$, the equation (2.20). The graph of the maximum and minimum values of L_{in_ϕ} was plotted as a function of the circuit power ($P_{3\phi}$) (Figure 18). As in the previous analysis, it is not possible to find a solution because, for all the power range, $L_{in_{\phi_{min}}} > L_{in_{\phi_{max}}}$

Changing the value of the transformer voltage ratio ($N = 1.0144$) it is found

Table 9 – Conditions for the calculation of $L_{in_{\phi_{min}}}$ and $L_{in_{\phi_{max}}}$ with variable frequency.

Variable	Symbol	Value	
		$L_{in_{\phi_{min}}}$	$L_{in_{\phi_{max}}}$
Supply rms phase voltage	V_{s_ϕ}	118 V	108 V
Limiting condition	-	Harmonics of I_s	$V_o = 250\,\text{V}$
Supply frequency	f	360 Hz	800 Hz

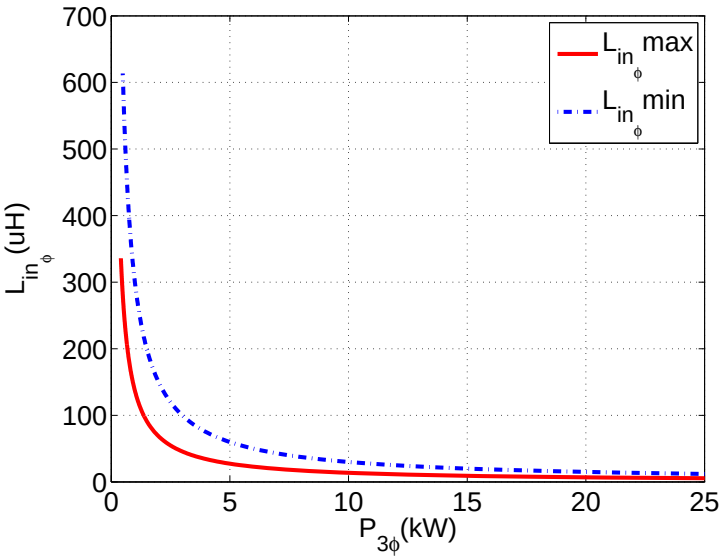

Figure 18 – Maximum and minimum value of the input inductor for variable frequency with N=1

the new graph of L_{in_ϕ} as a function of the circuit power (Figure 19). Similar to the fixed frequency, with N=1.0144, it is possible to find a value of L_{in_ϕ} that satisfies both conditions, for the rated power (25 kW), $L_{in_{\phi_{min}}} = 12.36\,\mu\text{H}$ and $L_{in_{\phi_{max}}} = 13.05\,\mu\text{H}$.

2.2.3.2 Circuit simulation at PLECS with variable frequency

Using the L_{in_ϕ} values found in the mathematical model, the circuit was simulated in the software PLECS. The circuit parameters are presented in Table 10 and the PLECS diagram is the same of the fixed frequency (Figure 15).

With the maximum value of the inductance ($L_{in_{\phi_{max}}} = 13.05\,\mu\text{H}$) it was analyzed the output voltage (Figure 20). According to the model the average output voltage is 250 V and in the simulation is 249.9 V.

The Figure 16 shows the output voltage with $L_{in_{\phi_{max}}}$ =13.05 µH. The average output voltage in the simulation is 249.9 V, which is really close to expected according to the mathematical model ($\overline{V_o} = 250\,\text{V}$).

Using $L_{in_{\phi_{min}}}$ =12.36 µH it is analyzed the harmonic content of the source

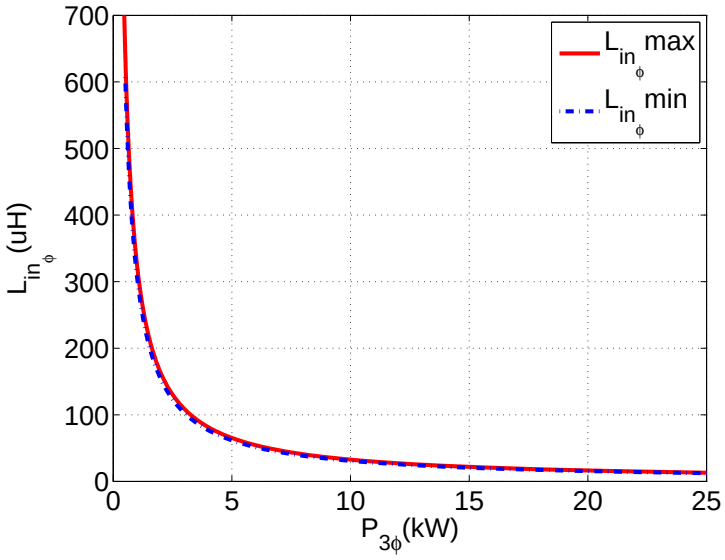

Figure 19 – Maximum and minimum value of the input inductor for variable frequency with N=1.0144.

Table 10 – Plecs simulation parameters with variable frequency - L filter.

Variable	Symbol	Value	
		$L_{in_{\phi_{min}}}$= 12.36 µH	$L_{in_{\phi_{max}}}$= 13.05 µF
Supply rms phase voltage	V_{s_ϕ}	118 V	108 V
Supply frequency	f	360 Hz	800 Hz
Output filter inductor	L_{out}	500 µH	
Output filter capacitor	C_{out}	200 µF	
Power in each rectifier	$P_{3\phi}$	25 kW	
Voltage ratio	N	1.0144	

current.The Figure 21 shows the waveform of the input current and Table 11 shows the comparison between the simulated and calculated values. As calculated in the previous section, these values meet the standards. Similar to the fixed frequency, the values are very close and the differences are due to the mathematical model assumes a constant output current while in the simulation the output current has a small ripple.

This section showed that the mathematical model is in agreement with the simulation results and that there is a feasible numerical value for L_{in_ϕ}. In the scenario of variable frequency the allowed inductance range is even smaller than in the fixed frequency. According to the data present in (GONG *et al.*, 2003; MINO *et al.*, 2005; GONG *et al.*, 2005; BAGHRAMIAN *et al.*, 2011; CHIVITE-ZABALZA; FORSYTH, 2005; CROSS *et al.*, 2009), this value is too small to be used in a real situation once the model is not considering losses, inductances of transformers, wires and generator and voltage drops in diodes. Therefore, it is necessary to explore other solutions to limit the harmonics of the

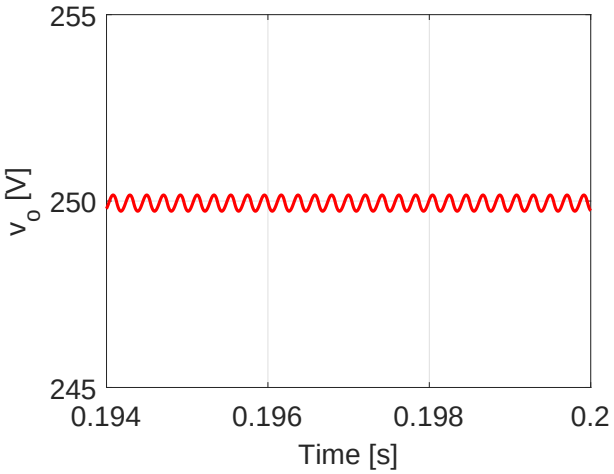

Figure 20 – Simulation output voltage with L filter - $L_{in_{\phi max}}$ =13.05 µH, f = 800 Hz and V_{s_ϕ} = 108 V.

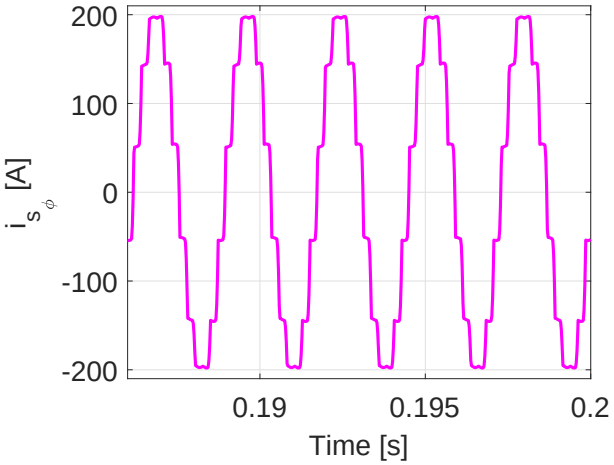

Figure 21 – Simulation input current with L filter - $L_{in_{\phi min}}$ =12.36 µH, f = 360 Hz and V_{s_ϕ} = 118 V.

Table 11 – Harmonic content of input current - comparison between the simulated and calculated values - $L_{in_{\phi min}}$ =12.36 µH, f = 360 Hz and V_{s_ϕ} = 118 V.

Harmonic order	Peak value - calculation (A)	Peak value - simulation (A)
11	16.076	16.251
13	12.977	12.621
23	5.095	5.114
25	4.244	4.269
35	1.695	1.720
37	1.442	1.479

input current.

2.3 Second order input LC filter

As shown in chapter 2.2, using only the L filter, the inductance value is not compatible with the real values of the circuit. The use of a second-order filter could produce a more efficient filtering, minimizing the commutation interval and allowing the use of larger inductors. The Figure 22 shows the complete circuit using the input LC filter. For the analysis, all the elements are considered ideal.

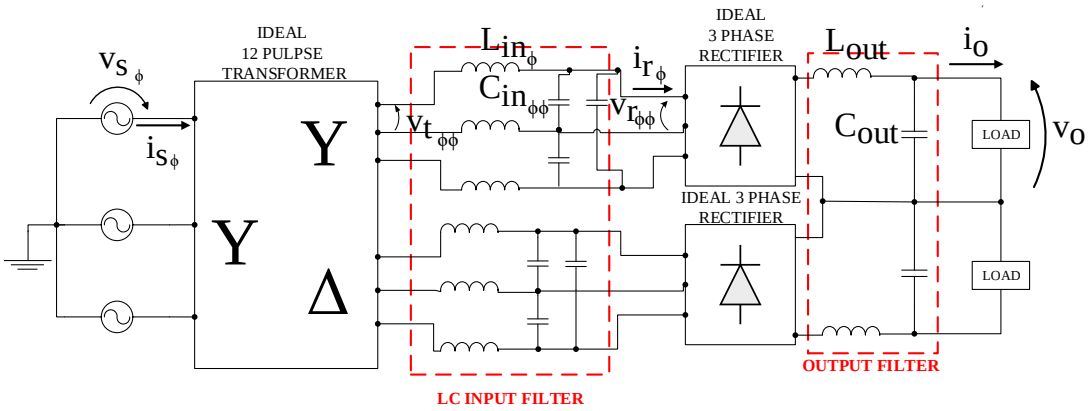

Figure 22 – Circuit using the input LC filter.

2.3.1 Mathematical modeling

The circuit must limit the harmonic input currents and should have an acceptable value of the load voltage. This section develops an approximate model of the circuit.

To model the circuit, the current at the input of the rectifier is analyzed (i_{r_ϕ}). Considering its fundamental value regards the ideal waveform (Figure 23), it is possible to write its Fourier series. The fundamental value is given by Equations (2.22), (2.23), (2.25) and (2.26).

$$i_{r_{\phi-1}}(\theta) = A_1 \cos(\theta) + B_1 \sin(\theta) \tag{2.22}$$

Where

$$A_1 = 0 \tag{2.23}$$

$$B_1 = \frac{\overline{I_o}}{\pi}\left[\frac{-\cos(\theta)}{1}\Bigg|_{30°}^{150°} + \frac{\cos(\theta)}{1}\Bigg|_{210°}^{330°}\right] \tag{2.24}$$

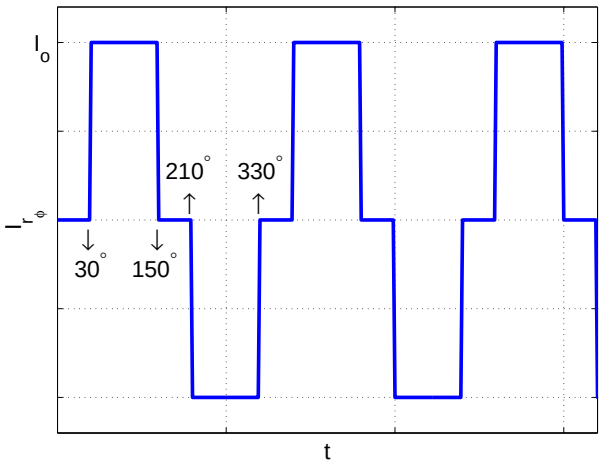

Figure 23 – Waveform to analyze the rectifier input current.

$$B_1 = \frac{2\sqrt{3I_o}}{\pi} \tag{2.25}$$

Therefore

$$i_{r_{\phi-1}}(\theta) = \frac{2\sqrt{3}I_o}{\pi} sin(\theta) \tag{2.26}$$

The total active power is entirely contained at the fundamental frequency (Equation (2.27)). Where $P_{1\phi}$ is the active power at one phase, $V_{s_{\phi-1}}$ is the RMS value of the source voltage, $I_{s_{\phi-1}}$ is RMS fundamental of the source current and Ψ_1 is the phase angle between $V_{s_{\phi-1}}$ and $I_{s_{\phi-1}}$.

$$P_{1\phi} = V_{s_{\phi-1}} I_{s_{\phi-1}} \cos(\Psi_1) \tag{2.27}$$

Once exists only a inductance between the source and the rectifier, the active power at the input of the rectifier can be written as Equation (2.28). Where $P_{1\phi}$ is the active power at one phase, $V_{r_{\phi-1}}$ is the fundamental voltage at the input of the rectifier and φ_1 is the phase angle between $V_{r_{\phi-1}}$ and $I_{r_{\phi-1}}$. For the harmonics the value of φ_1 is 90°, once a lossless circuit is being considered. Thus, the active power is entire at the fundamental.

$$P_{1\phi} = V_{r_{\phi-1}} I_{r_{\phi-1}} \cos(\varphi_1) \tag{2.28}$$

Moreover, $P_{1\phi} = P_o/3$, thereby, using (2.26) and (2.28), there is a relation

between $V_{r_{\phi-1}}$ and V_o:

$$\overline{V_o} = \frac{V_{r_{\phi-1}} \cos(\varphi_1) 6\sqrt{3}}{\sqrt{2}\pi} \tag{2.29}$$

Considering the equivalent impedance seen by the input filter ($Z_1 = V_{r_{\phi-1}}/I_{r_{\phi-1}}$) has a resistive part called R_1, the active power can be written as (2.30).

$$P_{1\phi} = R_1 I_{r_{\phi-1}}^2 \tag{2.30}$$

Using equations (2.28), (2.29) and (2.30), it is found a relation between $I_{r_{\phi-1}}$, $\overline{V_o}$ and R_1:

$$I_{r_{\phi-1}} = \frac{\overline{V_o}}{R_1} \frac{\pi\sqrt{2}}{6\sqrt{3}} \tag{2.31}$$

Equating the equations (2.26) and (2.31) and using $\overline{I_o} = P_{3\phi}/\overline{V_o}$ it is found a relation between R1 and $\overline{V_o}$:

$$R_1 = \overline{V_o}^2 \frac{\pi^2}{18 P_{3\phi}} \tag{2.32}$$

Thus, it is noticed that the output voltage can be found through $V_{r_{\phi-1}}$ and φ_1 (Equation (2.29)) or through R_1 (Equation (2.32)).

The appendix A presents a model to calculate the possible values of Z_1 (R_1 and X_1).

2.3.2 Input filter design

This section establishes a method for designing the input filter for both, fixed (400 Hz) and variable frequency (360 - 800 Hz).

The output value depends on $V_{r_{\phi-1}}$, which depends on the values of the input filter (L_{in_ϕ} and $C_{in_{\phi\phi}}$). Moreover, the harmonic input current also depends on the filter values.

The leakage inductance of the transformer and generator must be considered, as well the cables inductances. The use of the LC filter after the transformer (secondary side) allows to include such inductances on L_{in_ϕ}. If the filter was used at the transformer primary side, its leakage inductance would affect the system behavior similarly to the L filter analysis. From the data presented in (GONG *et al.*, 2003; MINO *et al.*, 2005; GONG *et al.*, 2005; BAGHRAMIAN *et al.*, 2011; CHIVITE-ZABALZA; FORSYTH, 2005;

CROSS *et al.*, 2009), the value of the total leakage inductance is around 300uH, for a 50 kW system.

In order to attenuate the harmonics of the input current, the filter cutoff frequency should be lower than the lowest harmonic liable to exist in the circuit withal it must be greater than the operating frequency.

The Figure 24 shows the phase diagram of the filter and the Figure 25 shows the Bode diagrams of V_{r_ϕ}/V_{t_ϕ} for rated and open circuit load. Moving closer to the resonance frequency, V_{r_ϕ} increases. The load attenuates this gain. It is important that any frequency that exists in the circuit coincides with the resonance frequency, if this occurs the value of V_{r_ϕ} would increase greatly, which would raise the output voltage. A damped filter could be used to attenuate this resonance, however this would imply in higher electrical losses, not justifying its use.

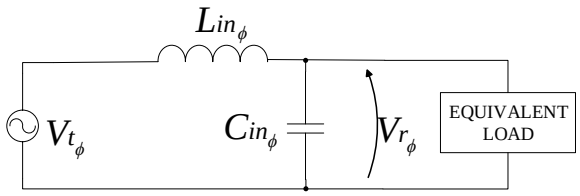

Figure 24 – Equivalent phase diagram with LC filter.

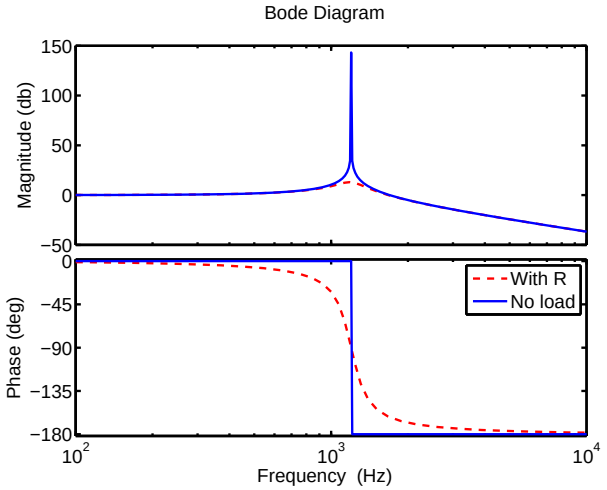

Figure 25 Bode diagram of V_{r_ϕ}/V_{t_ϕ} with and without a load resistor.

To calculate the relation between L_{in_ϕ} and C_{in_ϕ} it is analyzed the active power on the equivalent Thevenin circuit at the fundamental frequency (Figure 26). The values of the Thevenin voltage ($V_{th_{\phi-1}}$) and impedance ($X_{th_{\phi-1}}$) are calculated by (2.33) and (2.34), respectively (CLOSE, 1966). The subscript 1 indicates that it is the calculation

for the fundamental. w_r is the cutoff angular frequency of the filter and w is the angular frequency of the source.

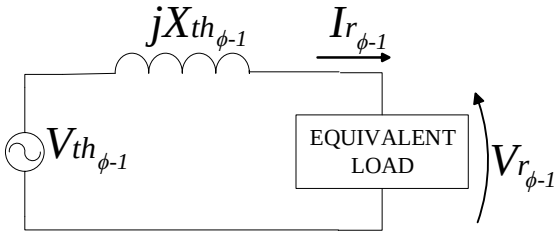

Figure 26 – Equivalent Thevenin circuit of LC input filter.

$$V_{th_{\phi-1}} = V_{t_{\phi-1}} \frac{w_r^2}{w_r^2 - w^2} \tag{2.33}$$

$$X_{th_{\phi-1}} = L_{in_\phi} \frac{w_r^2 w}{w_r^2 - w^2} \tag{2.34}$$

At first, the equivalent load is modeled as a resistance (R_1), once the circuit without harmonics results in phase current and voltage at the rectifier input, even with some harmonic contents, this phase difference should not be large.

The maximum power that can be delivered occurs for $R_1 = X_{th_{\phi-1}}$ (CLOSE, 1966), therefore, the value of L_{in_ϕ} to supply the maximum power is given by (2.38). Following is the method to find the Equation (2.38). The Equation (2.39) gives the capacitor value.

$$P_{1\phi} = \frac{V_{r_{\phi-1}}^2}{R_1} \tag{2.35}$$

For the maximum power $R_1 = X_{th_{\phi-1}}$:

$$P_{max_{1\phi}} = \frac{V_{r_{\phi-1}}^2}{\left|X_{th_{\phi-1}}\right|} = \frac{\left|V_{th_{\phi-1}}\right|^2}{2\left|X_{th_{\phi-1}}\right|} \tag{2.36}$$

Replacing the values of $V_{th_{\phi-1}}$ and $X_{th_{\phi-1}}$:

$$L_{in_\phi} = \frac{V_{t_{\phi-1}}^2 w_r^2}{2wP_{max_{1\phi}}} \left|\frac{1}{w_r^2 - w^2}\right| \tag{2.37}$$

$$L_{in_\phi} = \frac{(NV_{s_\phi})^2 w_r^2}{2wP_{max_{1\phi}}} \left|\frac{1}{w_r^2 - w^2}\right| \tag{2.38}$$

$$C_{in_\phi} = \frac{1}{L_{in_\phi} w_r^2} \tag{2.39}$$

The output power is limited by the value of L_{in_ϕ} thus, it is possible to establish the maximum value of L_{in_ϕ} with the worst operation conditions for this situation: minimum value of the voltage source and maximum frequency. Using these conditions, and the filter cutoff frequency previously selected, it is possible to find the values of L_{in_ϕ} and C_{in_ϕ} using equations (2.38) and (2.39).

2.3.3 Analysis of the circuit operating with fixed frequency (400 Hz)

First, it will be analyzed how the circuit behaves operating at a fixed frequency (400 Hz).

2.3.3.1 Input filter design

As explained at section 2.3.2, in order to attenuate the harmonics of the input current, the filter cutoff frequency should be lower than the lowest harmonic liable to exist in the circuit (5^{th} harmonic of 400 Hz - 2000 Hz) withal it must be greater than the operating frequency (400 Hz). Thereby, 1400 Hz was chosen as the cutoff frequency of the filter.

Considering $P_{max_{1\phi}} = P_{3\phi}/3 = 25/3$ kW and the limits establish by equation (2.38) and (2.39), $L_{in_\phi} = 330\,\mu H$ and $C_{in_\phi} = 13.05\,\mu F$. The L_{in_ϕ} value is close to the typical leakage inductances of the system, therefore, this value is liable to be used. The capacitor value was found directly by the equations, but it is not a commercial value.

2.3.3.2 Simulation results

With the input filter values calculated in the previous section, the circuit was simulated in the software PLECS (Figure 27). The parameters are present in Table 12.

The Figure 28 shows the waveforms of the voltage and current at the source with $V_{s_\phi} = 108\,V$ and $V_{s_\phi} = 118\,V$. Figure 29 and Table 13 show the current spectra in the source and in the output of the transformer (I_{t_ϕ}). As can be seen, the harmonic limits of the source current are respected. For I_{t_ϕ} it is observed high values close to the filter resonance (1400 Hz), although the 5^{th} and 7^{th} harmonics are eliminated in the primary, this effect is not felt by the source (Figure 29).

The Figure 30 shows the voltage at the rectifier output (v_{dc}) and at the load (v_o and i_o) with $V_{s_\phi} = 108\,V$ and $V_{s_\phi} = 118\,V$. As can be seen, the ripple of the load voltage remains within the limits established by the standard. For $V_{s_\phi} = 108\,V$ the average load voltage is within the limits of the standard. $V_{s_\phi} = 118\,V$ this value is slightly above the

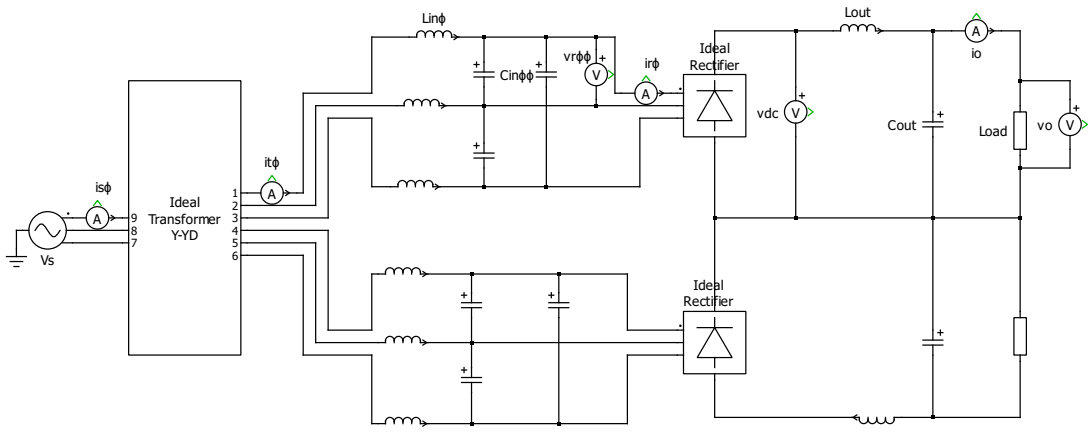

Figure 27 – Circuit diagram at PLECS software with the LC input filter.

Table 12 – PLECS simulation parameters - LC filter with constant frequency.

Variable	Symbol	Value
Output power in each rectifier	P_o	25 kW
Supply rms phase voltage	V_{s_ϕ}	108 V and 118 V
Supply frequency	f	400 Hz
Voltage ratio	N	1
Input filter inductor	L_{in_ϕ}	330 µH
Input filter capacitor (Δ connection)	$C_{in_{\phi\phi}}$	13.05 µF
Output filter inductor	L_{out}	500 µH
Output filter capacitor	C_{out}	200 µF

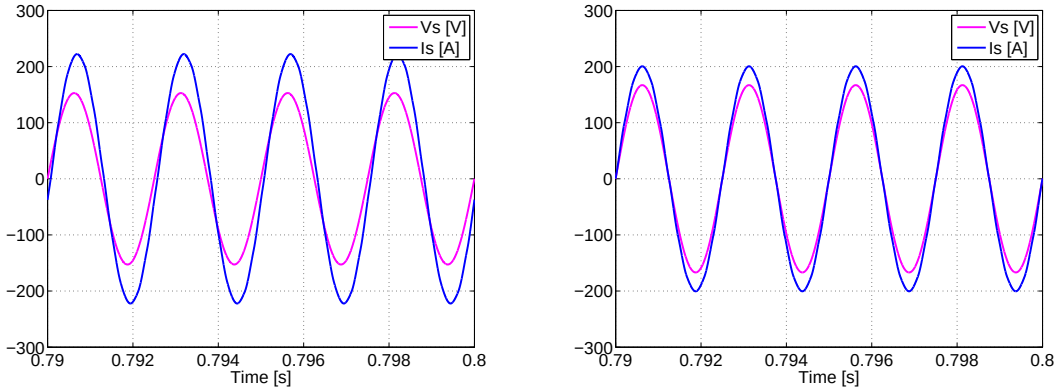

(a) $V_{s_\phi} = 108\,\text{V}$ (b) $V_{s_\phi} = 118\,\text{V}$

Figure 28 – Current (blue) and voltage(magenta) at source with $f = 400\,\text{Hz}$.

allowed, however the real circuit presents voltage drops that are not considered in this model. Thus this value probably will comply with the standard.

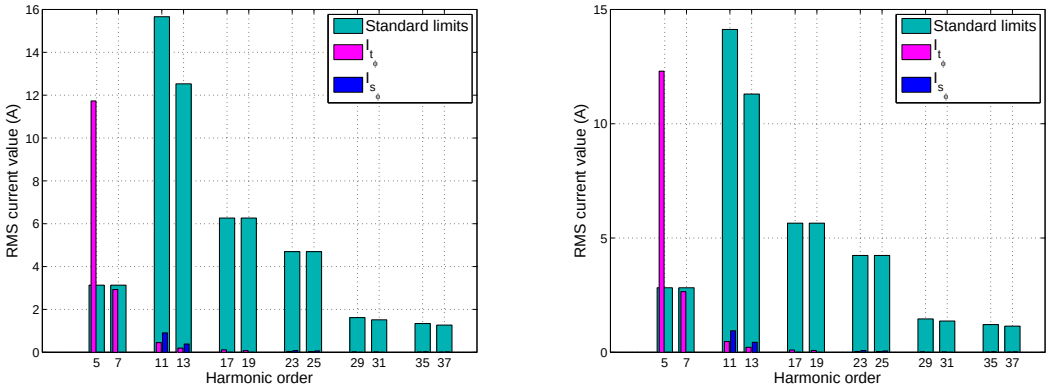

(a) $V_{s_\phi} = 108\,\text{V}$ (b) $V_{s_\phi} = 118\,\text{V}$

Figure 29 – Harmonic spectra of the current in the source (dark blue), in the output of the transformer (magenta) and the standard limits (light blue) with $f = 400\,\text{Hz}$.

Table 13 – Numeric values of the Figure 29 - Harmonic spectra of the current in the source (dark blue), in the output of the transformer (magenta) and the standard limits (light blue) with $f = 400\,\text{Hz}$.

	$V_{s_\phi} = 108\,\text{V}$		$V_{s_\phi} = 118\,\text{V}$	
Harmonic order	I_{s_ϕ} (A)	I_{t_ϕ} (A)	I_{s_ϕ} (A)	I_{t_ϕ} (A)
5	0	11.73	0	12.3
7	0	2.93	0	2.65
11	0.9	0.45	0.94	0.47
13	0.38	0.19	0.44	0.22
17	0	0.11	0	0.10
19	0	0.07	0	0.08
23	0.06	0.03	0.06	0.03
25	0.06	0.03	0.06	0.03
29	0	0.01	0	0.02
31	0	0.01	0	0.01
35	0.02	0.01	0.02	0.01
37	0	0	0	0

The Figure 31 shows the voltage (v_{r_ϕ}) and current (i_{r_ϕ}) at the input of the rectifiers and Figure 32 and Table 14 show the harmonic spectra of v_{r_ϕ} with $V_{s_\phi} = 108\,\text{V}$ and $V_{s_\phi} = 118\,\text{V}$. As can be seen, the harmonic content for both voltages is similar once the source frequency is the same, for $V_{s_\phi} = 118\,\text{V}$, the fundamental value of V_{r_ϕ} is higher, which makes the output voltage is slightly higher than V_{s_ϕ} as well (Figure 30).

The Table 15 shows the simulation fundamental values of $V_{r_{\phi-1}}$ and $I_{r_{\phi-1}}$, the equivalent impedance seen by the input filter ($Z_1 = V_{r_{\phi-1}}/I_{r_{\phi-1}}$) and the angle between $V_{r_{\phi-1}}$ and $I_{r_{\phi-1}}$ (φ_1). As shown in the table, the impedance seen by the input filter (Z_1) is not purely resistive. This happens due to the presence of harmonics in the voltage that cause the diodes switching moment to be advanced or delayed.

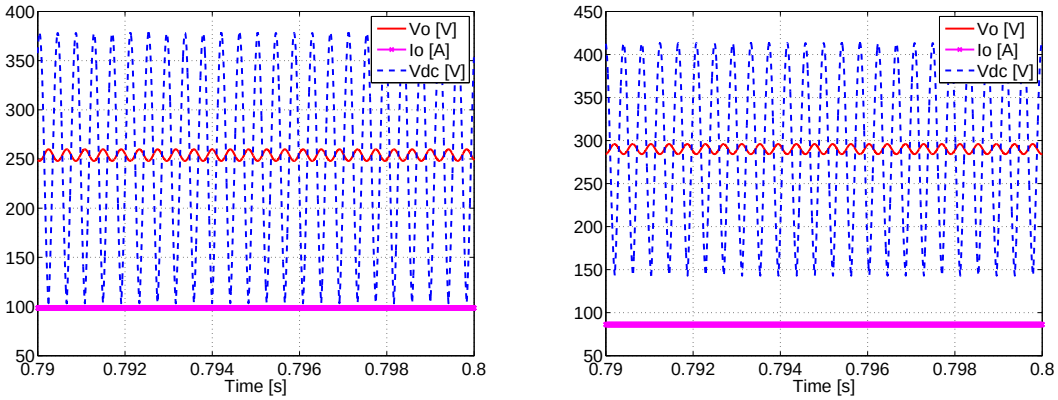

(a) $V_{s_\phi} = 108\,\mathrm{V}$ (b) $V_{s_\phi} = 118\,\mathrm{V}$

Figure 30 – Voltage at the output of the rectifier (blue), load current (magenta) and load voltage (red) with $f = 400\,\mathrm{Hz}$.

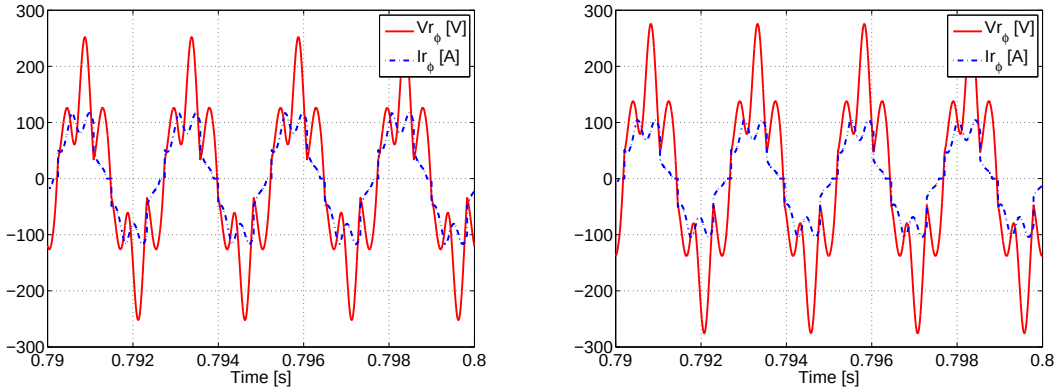

(a) $V_{s_\phi} = 108\,\mathrm{V}$ (b) $V_{s_\phi} = 118\,\mathrm{V}$

Figure 31 – Current (blue) and voltage (red) at the input of the rectifier with $f = 400\,\mathrm{Hz}$.

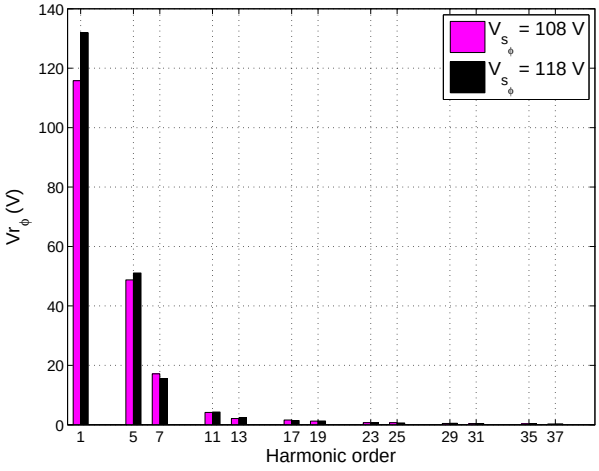

Figure 32 – Voltage spectra at the input of the rectifier – RMS value with $f = 400\,\mathrm{Hz}$, $V_{s_\phi} = 108\,\mathrm{V}$ and $V_{s_\phi} = 118\,\mathrm{V}$.

Table 14 – Numeric values of the Figure 32 - Voltage spectra at the input of the rectifier – RMS value with $f = 400\,\text{Hz}$, $V_{s_\phi} = 108\,\text{V}$ and $V_{s_\phi} = 118\,\text{V}$.

Harmonic order	$V_{s_\phi} = 108\,\text{V}$	$V_{s_\phi} = 118\,\text{V}$
1	115.79	131.93
5	48.76	51.07
7	17.15	15.51
11	4.15	4.29
13	2.11	2.38
17	1.62	1.44
19	1.23	1.26
23	0.73	0.72
25	0.70	0.62
29	0.45	0.51
31	0.40	0.41
35	0.35	0.33
37	0.28	0.31

Table 15 – Simulation values of $V_{r_{\phi-1}}$, $I_{r_{\phi-1}}$, Z_1 and φ_1 at the fundamental frequency with $f = 400\,\text{Hz}$.

V_{s_ϕ}	108 V	118 V
$V_{r_{\phi-1}}$	115.63 $\angle -33.6°$	131.85 $\angle -26.3°$
$I_{r_{\phi-1}}$	74.7 $\angle -18.4°$	65.87 $\angle -10.0°$
Z_1	1.49 -j0.41	1.92 -j0.56
φ_1	-15.2°	-16.3°

Since it is a nonlinear circuit, the value of φ_1 or R_1 can be obtained only through simulations. Using the values of Table 15 in equation 2.32, it is possible to compare the results from the simulation with the expected by the model. The Table 16 shows this comparative and, as can be seen, the values are close, i.e., this model provides a good approximation of the value of $\overline{V_o}$, once it is known the value of R_1.

Table 16 – Comparison of the $\overline{V_o}$ value obtained by the mathematical model and by simulation with $f = 400\,\text{Hz}$.

V_{s_ϕ} =108 V			V_{s_ϕ} =118 V		
	Calculated	Simulated		Calculated	Simulated
V_o	260.65 V	253.83 V	V_o	295.87 V	289.80 V

Independent of the input filter or the operating frequency, another point to be analyzed is when the circuit power tends to zero. When this occurs, the output voltage tends to the peak value of the source line voltage, since the capacitor charges at its

maximum and does not discharge. In this situation the output voltage exceeds the limits of the standard with $V_{s_\phi} = 118\,\text{V}$ because $\overline{V_o}$ tends to 289 V and, as the current tends to zero, the voltage drops are negligible. This fact indicates the standards should reconsider the voltage specification limits.

This section showed that with the LC filter and constant frequency it is possible to increase the inductor value to levels appropriate to the application. Also it is possible to meet the standard limits if it considers that there are small voltage drops that are not being considered in the model.

2.3.4 Analysis of the circuit operating with variable frequency (360 - 800 Hz)

2.3.4.1 Filter design

The filter design follow the same methodology from section 2.3.2. The resonance frequency should be lower than the lowest harmonic liable to exist in the circuit ($h_{min} * f_{min} = 5^{th}$ harmonic of 360 Hz - 1800 Hz) withal it must be greater than the maximum operating frequency (800 Hz). Thereby, 1200 Hz was chosen as the cutoff frequency of the filter. It is worth mentioning that this frequency range is very small.

The Figure 33 shows the Bode diagram of V_{r_ϕ}/V_{t_ϕ} for two conditions: with the equivalent load modeled as a resistor and with no load. As can be seen, moving closer to the resonance, V_{r_ϕ} increases. With the load this gain is attenuated. As the source frequency can assume any value between 360 Hz and 800 Hz, if the resonance was adjusted above 1800 Hz it would exist an operating frequency with a harmonic component at 1800 Hz which would lead the circuit to a probable over voltage.

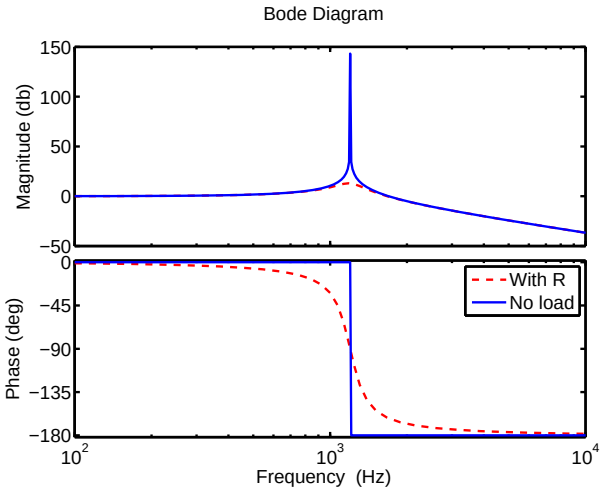

Figure 33 Bode diagram of V_{r_ϕ}/V_{t_ϕ} with and without a load resistor.

With $P_{max_{1\phi}} = P_{3\phi}/3 = 25/3$ kW, the cutoff frequency selected above and the limits establish by equations (2.38) and (2.39), $L_{in_\phi} = 250.6\,\mu\text{H}$ and $C_{in_{\phi\phi}} = 23.39\,\mu\text{F}$.

The L_{in_ϕ} value is close to the typical leakage inductances of the system, therefore, this value is liable to be used. The capacitor value was found directly by the equations, but it is not a commercial value.

2.3.4.2 Simulation results

The circuit was simulated at PLECS software (Figure 27) with the data of Table 17.

Table 17 – PLECS simulation parameters - LC filter with variable frequency.

Variable	Symbol	Value
Output power in each rectifier	P_o	25 kW
Supply rms phase voltage	V_{s_ϕ}	108 V and 118 V
Voltage ratio	N	1
Input filter inductor	L_{in_ϕ}	250.6 µH
Input filter capacitor (Δ connection)	$C_{in_{\phi\phi}}$	23.39 µF
Output filter inductor	L_{out}	500 µH
Output filter capacitor	C_{out}	200 µF

The current source (i_{s_ϕ}) is analyzed only with $V_{s_\phi} = 118$ V, since this configuration presents the higher harmonic currents. The Figure 34 shows the voltage and current at the source for both frequencies and Figure 35 and Table 18 show the current spectra at the source and at the output of the transformer (i_{t_ϕ}). As can be seen, the harmonic limits of the source current are respected for both frequencies. With the circuit operating at 360 Hz, the 5^{th} and 7^{th} (1800 Hz e 2520 Hz) harmonics of i_{t_ϕ} are greatly amplified, this happens because these frequencies are close to the cutoff frequency of the filter (1200 Hz) and the resonance phenomenon occurs. However, the 5^{th} and 7^{th} harmonics are eliminated in the primary so this effect is not felt by the source as shown in Figure 35. It is worth mentioning that this current is flowing through a part of the circuit and therefore, when dimensioning the equipments and components it should be taken into consideration.

The Figure 36 shows the voltage at the rectifier output (v_{dc}) and at the loads (v_o and i_o) for $V_{s_\phi} = 118$ V and both frequencies. The Table 19 shows the average output voltage for all the circuit situations: with limits of source frequency ($f = 360$ Hz and $f = 800$ Hz) and with limits of voltage source ($V_{s_\phi} = 108$ V and $V_{s_\phi} = 118$ V).

Although the ripple is within the limits established by the standard, the average load voltage exceeds the standard limit (280 V) for almost all situations. This appears due to the resonance effect of the input filter.

To better understand the resonance effect, the voltage at the rectifier input is analyzed. The Figure 37 shows current and voltage waveforms at the rectifier input and Figure 38 shows the spectra of v_{r_ϕ} with the maximum value of Vs (118 V). The Table

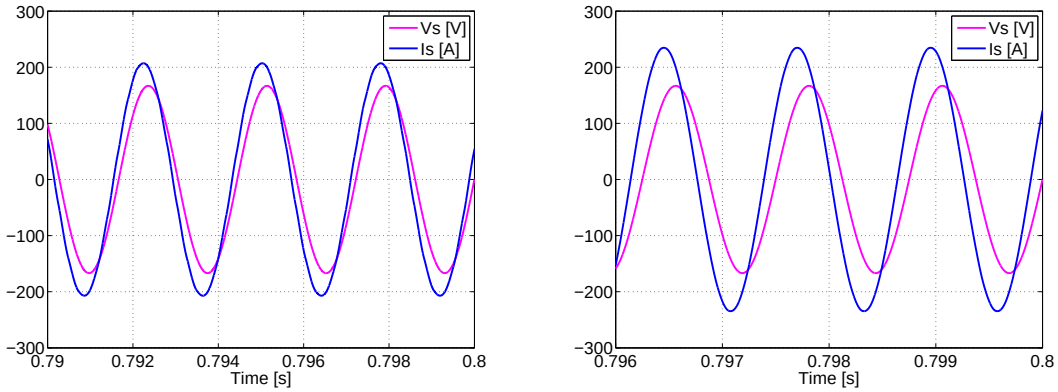

(a) $f = 360\,\text{Hz}$ (b) $f = 800\,\text{Hz}$

Figure 34 – Current (blue) and voltage(magenta) at source with $V_{s_\phi} = 118\,\text{V}$.

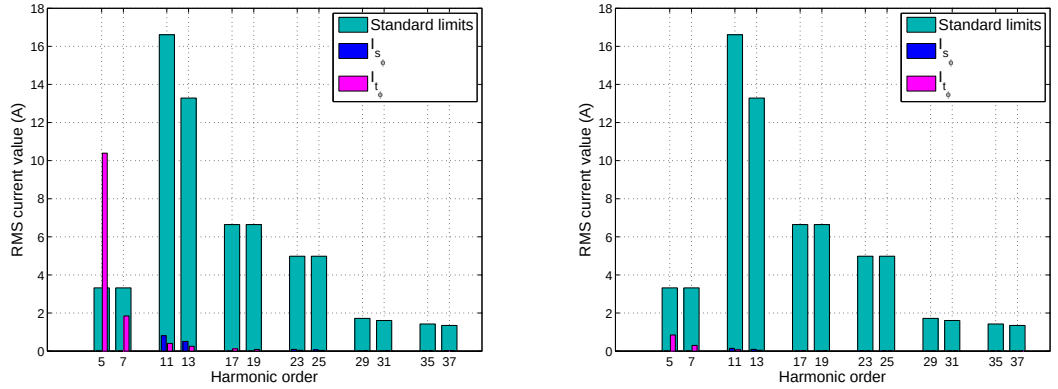

(a) $f = 360\,\text{Hz}$ (b) $f = 800\,\text{Hz}$

Figure 35 – Current spectra of current in the source (dark blue), in the output of the transformer (magenta) and the standard limits (light blue) with $V_{s_\phi} = 118\,\text{V}$.

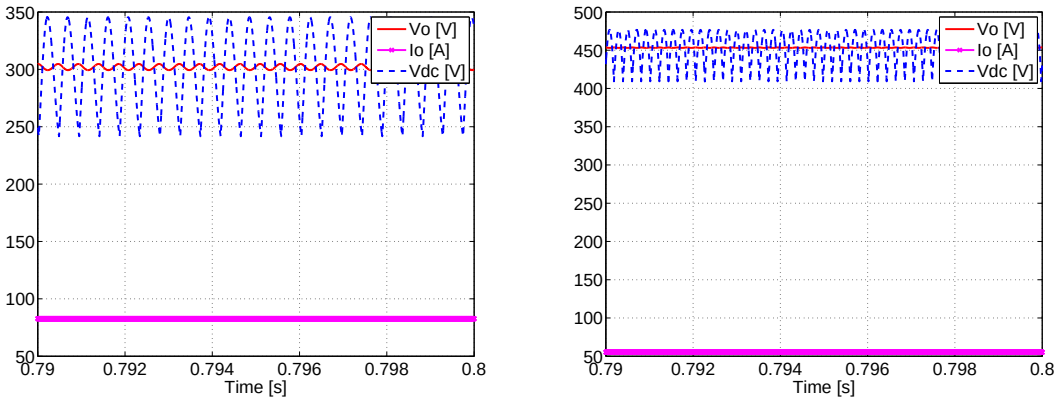

(a) $f = 360\,\text{Hz}$ (b) $f = 800\,\text{Hz}$

Figure 36 – Voltage at the output of the rectifiers (blue), load current (magenta) and load voltage (red) with $V_{s_\phi} = 118\,\text{V}$.

Table 18 – Numeric values of the Figure 35 - Current spectra of current in the source (dark blue), in the output of the transformer (magenta) and the standard limits (light blue) with $V_{s_\phi} = 118\,\text{V}$.

	$f = 360\,\text{Hz}$		$f = 800\,\text{Hz}$	
Harmonic order	I_{s_ϕ}	I_{t_ϕ}	I_{s_ϕ}	I_{t_ϕ}
5	0	10.39	0	0.85
7	0	1.84	0	0.3
11	0.8	0.40	0.14	0.07
13	0.5	0.25	0.08	0.04
17	0	0.12	0	0.02
19	0	0.09	0	0.01
23	0.1	0.05	0.02	0.01
25	0.06	0.03	0.02	0.01
29	0	0.02	0	0
31	0	0.02	0	0
35	0.02	0.01	0	0
37	0.02	0.01	0	0

Table 19 – PLECS simulation values of $\overline{V_o}$.

		V_{s_ϕ}	
		108 V	118 V
f	360 Hz	274.4 V	301.9 V
	800 Hz	390.1 V	453.3 V

21 shows the simulation fundamental values of $V_{r_{\phi-1}}$ and $I_{r_{\phi-1}}$, the equivalent impedance seen by the input filter ($Z_1 = V_{r_{\phi-1}}/I_{r_{\phi-1}}$) and the angle between $V_{r_{\phi-1}}$ and $I_{r_{\phi-1}}$ (φ_1) for all operation cases.

As can be seen in Figure 37a, for 360 Hz, the current and voltage are more distorted, this occurs because the resonance frequency of the filter (1200 Hz) is close to the 5^{th} harmonic (1800 Hz). In Figure 38 this increase in the 5^{th} harmonic is clearly observed. This distortion changes the switching moment of the rectifier and causes a lag between the voltage and current at the fundamental (φ_1) (Table 21).

For 800 Hz, the harmonic content is lower (Figure 37b, 38 and Table 20) once the filter resonance frequency is farther from the harmonic frequencies present in the circuit. As a result, the shifting of the commutation point is smaller (Table 21). However, the fundamental value is amplified by the input filter since the frequency of 800 Hz is close to the cutoff frequency of the filter (1200 Hz), what increases the output voltage ($\overline{V_o}$).

As showed in Table 21 the impedance seen by the input filter is not purely resistive, it has a a reactive part. Using the model developed in the previous section to

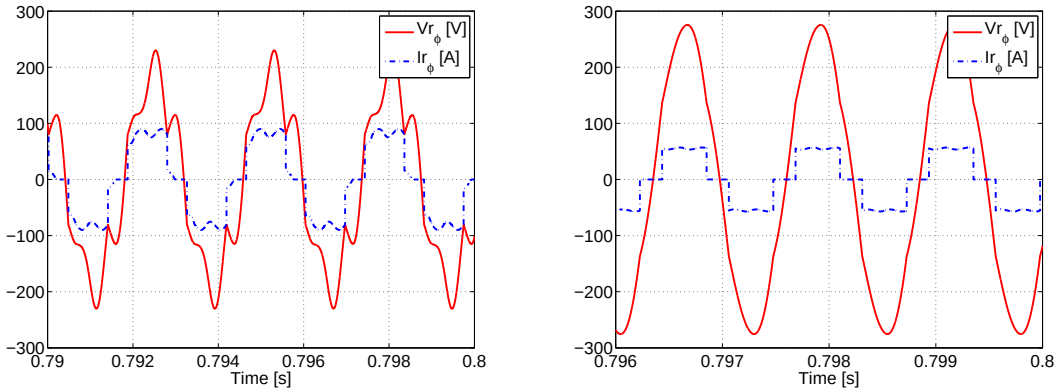

(a) $f = 360\,\text{Hz}$ (b) $f = 800\,\text{Hz}$

Figure 37 – Current (blue) and voltage (red) at the input of the rectifier with $V_{s_\phi} = 118\,\text{V}$.

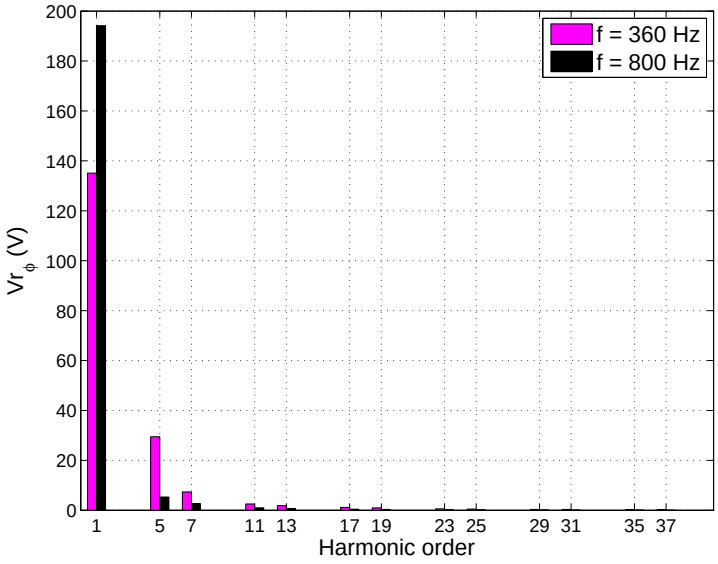

Figure 38 – Voltage spectra at the input of the rectifier – RMS value with $V_{s_\phi} = 118\,\text{V}$.

calculate the output voltage (Equation 2.32) with the data from the Table 21, it is possible to compare the values obtained by the simulation and by calculation (Table 22). As can be seen, the results are very close. Thus, knowing the value of R_1, it is possible to estimate the DC voltage value. At Figure 39, using the PLECS software, the operating frequency of the circuit was discreetly changed observing the behavior of the output voltage for $V_{s_\phi} = 118\,\text{V}$. As expected, the output voltage increases with increasing frequency. The peaks in the output voltage are due to instantaneous change in the source frequency.

Using the mathematical model it is possible to plot the value of V_{r_ϕ} as a function of R_1 and X_1 (Figure 40). As can be seen, the value of X_1 does not strongly interfere in V_{r_ϕ}. For 800 Hz, there is an increase in the V_{r_ϕ} compared to 360 Hz when the power increases (higher values of R_1). The value of the output voltage is directly related with V_{r_ϕ}.

Table 20 – Numeric values of the Figure 38 - Voltage spectra at the input of the rectifier – RMS value with $V_{s_\phi} = 118\,\text{V}$.

Harmonic order	$f = 360\,\text{Hz}$	$f = 360\,\text{Hz}$
1	135.06	194.15
5	29.48	5.34
7	7.35	2.65
11	2.54	1.03
13	1.88	0.73
17	1.18	0.42
19	0.95	0.34
23	0.61	0.23
25	0.49	0.2
29	0.37	0.14
31	0.33	0.13
35	0.27	0.1
37	0.23	0.09

Table 21 – Simulation values of $V_{r_{\phi-1}}$, $I_{r_{\phi-1}}$, Z_1 and φ_1 at the fundamental frequency.

$V_{s_\phi} = 108\,\text{V}$			$V_{s_\phi} = 118\,\text{V}$		
	360 Hz	800 Hz		360 Hz	800 Hz
$V_{r_{\phi-1}}$	123.17 $\angle -20.75°$	167.35 $\angle -35.41°$	$V_{r_{\phi-1}}$	135.065 $\angle -17.19°$	194.15 $\angle -27.2°$
$I_{r_{\phi-1}}$	70.45 $\angle -4.54°$	49.96 $\angle -30.72°$	$I_{r_{\phi-1}}$	64.29 $\angle -0.88°$	42.99 $\angle -23.88°$
Z_1	1.68 -j0.49	3.34 -j0.27	Z_1	2 -j0.59	4.51 -j0.26
φ_1	-16.21°	-4.69°	φ_1	-16.31°	-3.32°

Table 22 – Comparison of the V_o value obtained by calculation and by simulation.

$V_{s_\phi} = 108\,\text{V}$			$V_{s_\phi} = 118\,\text{V}$		
	Calculated (V)	Simulated (V)		Calculated (V)	Simulated (V)
360 Hz	276.76	274.37	360 Hz	301.97	301.92
800 Hz	388.48	390.1	800 Hz	453.47	453.34

With the LC filter it is possible to increase the value of the input inductor. Although, as the circuit operates over a wide range of frequencies, it is not possible to properly tune the filter to not interfere with any harmonic frequency. Therefore, even by choosing the cutoff frequency that produces the smallest resonance effect, the value of the output voltage still exceeds the allowed by the standard.

In order to reduce the voltage amplification due to the LC filter resonance excitation, a damping filter could be used. However, a resistive damping would increase

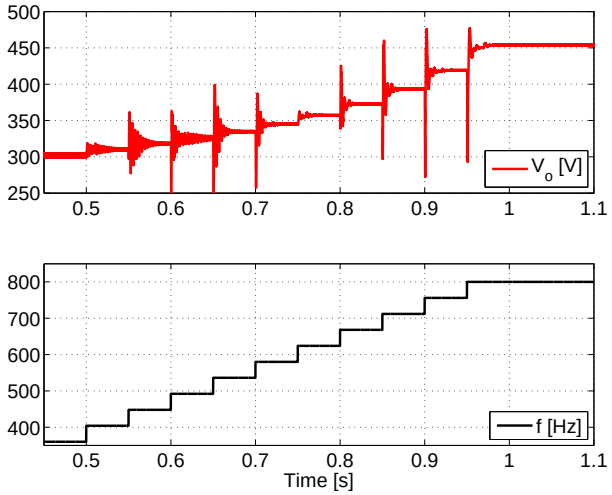

Figure 39 – Behavior of output voltage with frequency variation - PLECS sotware - $V_{s_\phi} = 118\,\text{V}$.

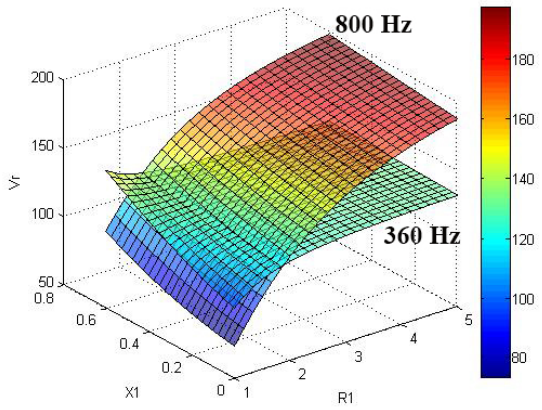

Figure 40 – Graph of V_{r_ϕ} as a function of R_1 and X_1.

the converter losses, affecting the overall efficiency, what is not technically sound for this application. To illustrate how this solution would be, it was designed a damped filter. The Figure 41 shows the phase diagram of the filter. The L_{in_ϕ} and C_{in_ϕ} values are the same as previously calculated, C_{d_ϕ} was chosen to be five times greater than the value of C_{in_ϕ} and the R_{in_ϕ} value was designed to limit the peak value of the resonance, making the gain as close to 1 as possible. Table 23 shows all the simulated values used.

Figure 42 shows the load voltage and Figure 43 shows the waveform and spectrum of the rectifier input voltage. By comparing with the analysis of the non-damping filter (Table 19, Figure 37 and Figure 38), it was seen that the output voltage was less amplified, the average output voltage with the damping filter is 257.8 V and with the non-damping filter is 274.4 V. This is due to the attenuation in the resonance peak, the Figure 43 shows this effect, as can been seen, the harmonic values are smaller than in the previous analysis.

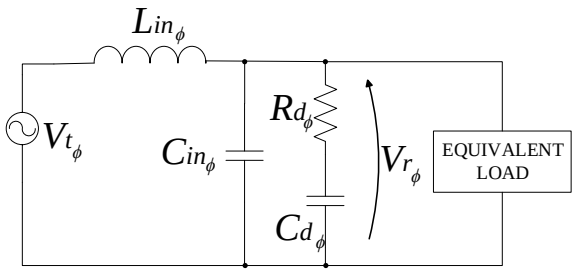

Figure 41 – Equivalent phase diagram with LC damping filter.

Table 23 – PLECS simulation parameters - LC damping filter.

Variable	Symbol	Value
Output power in each rectifier	P_o	25 kW
Supply rms phase voltage	V_{s_ϕ}	108 V
Supply frequency	f	360 Hz
Voltage ratio	N	1
Input filter inductor	L_{in_ϕ}	250.6 µH
Input filter capacitor (Δ connection)	$C_{in_{\phi\phi}}$	23.39 µF
Damping capacitor (Δ connection)	$C_{d_{\phi\phi}}$	117 µH
Damping resistor (Δ connection)	$R_{in_{\phi\phi}}$	8 Ω
Output filter inductor	L_{out}	500 µH
Output filter capacitor	C_{out}	200 µF

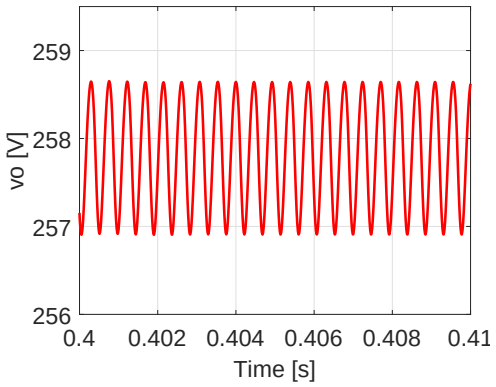

Figure 42 – Output voltage with an LC damping filter - $V_{s_\phi} = 108$ V and $f = 360$ Hz.

However, the use of damping filter causes high losses for this system. The output power is 25 kW and the source power is 37.7 kW, thus the yield of the system is 0.66, which is unacceptable. Active (electronic) damping solutions could be considered (GUERREIRO *et al.*, 2013), but such possibilities are out of the scope.

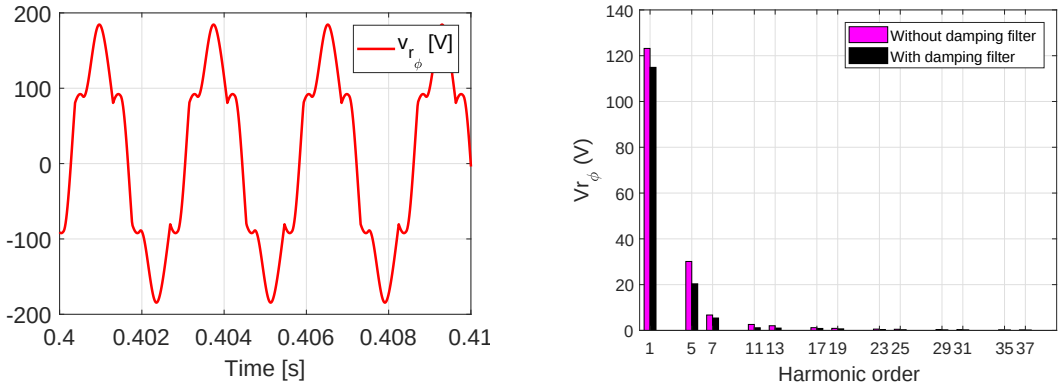

(a) Voltage waveform

(b) Harmonic spectra

Figure 43 – Input voltage of the rectifier with LC damping filter - $V_{s_\phi} = 108$ V and $f = 360$ Hz.

2.4 Conclusion

In this chapter, the 12-pulse rectifier with L and LC input filter was analyzed for fixed (400 Hz) and variable frequency (360 - 800 Hz) scenarios. The aim is to comply with aeronautical standards with respect to the harmonic content of the input current and the limits of the output voltage. A mathematical model and simulation were developed.

All results are in agreement, which shows that the mathematical model is robust and its use is valid. Using the L filter it is possible to achieve adequate DC voltages and comply with the standards, nonetheless the inductor must be very small, this restriction made this solution impracticable. With the LC filter, it is possible to increase the value of the input inductor and, with constant frequency operation, it is possible to tune the filter in order to comply with the standards. Although, with variable frequency, due to the wide range of frequency, it is not possible to properly tune the filter to not interfere with any harmonic frequency.

3 Prototype

3.1 First order input L filter

A prototype was assembled to verify the analysis performed previously (Figure 44). For the sake of simplicity, only one arm of the 12 pulse-rectifier was tested. With this configuration the 5^{th} and 7^{th} harmonics of the input current are not cancelated, but as this phenomenon has been widely studied in the literature (MOHAN *et al.*, 2003), the focus of the analysis is at the output voltage behavior for different frequencies.

The tests were done in a small scale for 360-800 Hz with the data present in Table 24. The value of the input inductor was chosen taking into account the prototype power and according to the availability in the laboratory. The output filter values have been chosen to attenuate the harmonics in the DC side and according to the available components. In addition, the tests were performed with resistive load and not with constant power as the previous analysis.

With these components and $V_{s_\phi} = 118\,\text{V}$, the total power was around 1500 W, this value correspond to approximately 6% of the rated power previously analyzed. In order to have an adequate comparison parameter, the circuit was simulated with the experimental data (Table 24) at the PLECS software. The voltage source used was the 345 - ASX from Pacific Power Source and the diode bridge used was the SKD 62/12 from Semikron.

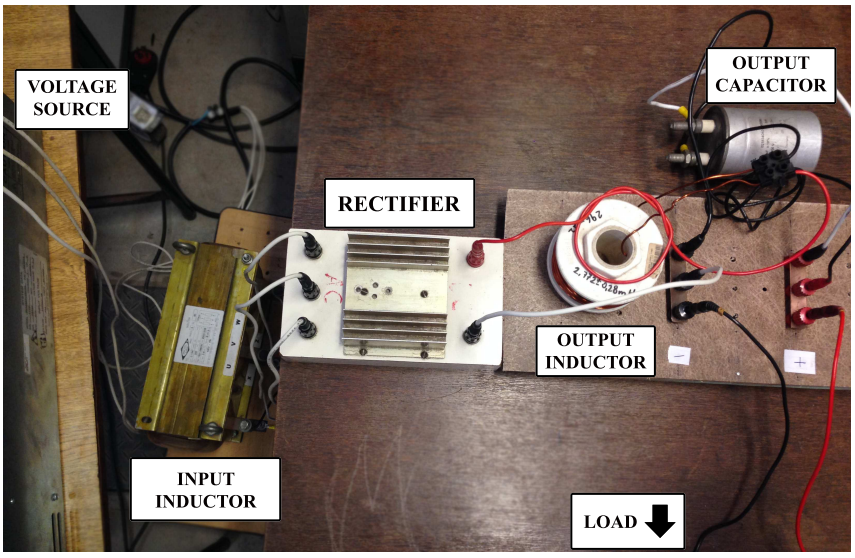

Figure 44 – Prototype with L input filter.

Figure 45 shows the input current obtained by simulation and by prototype,

Table 24 – Prototype parameters.

Variable	Symbol	Value
Supply rms phase voltage	V_{s_ϕ}	108 - 118 V
Supply frequency	f	360 - 800 Hz
Input filter inductor	L_{in_ϕ}	134 µH
Output resistor load	R_o	48 Ω
Output filter inductor	L_{out}	2.77 mH
Output filter capacitor	C_{out}	33 µF
Cutoff frequency of the output filter	f_c	526 Hz

with $V_{s_\phi} = 118$ V.As can be seen, the waveforms are visually similar. Figure 46 shows the simulation and prototype harmonic spectra of i_{s_ϕ}. Due to the attenuations present in the circuit that are not considered in the simulation, the prototype values are smaller than in the simulation. However, these simulation values are used to calculate the minimum value of the input inductor. Thus, using the model developed in section 2.2.1, the calculation is being conservative and ensures that the constraints of the standard will be met. Since the transformer was not used, the 5^{th} and 7^{th} harmonics appear.

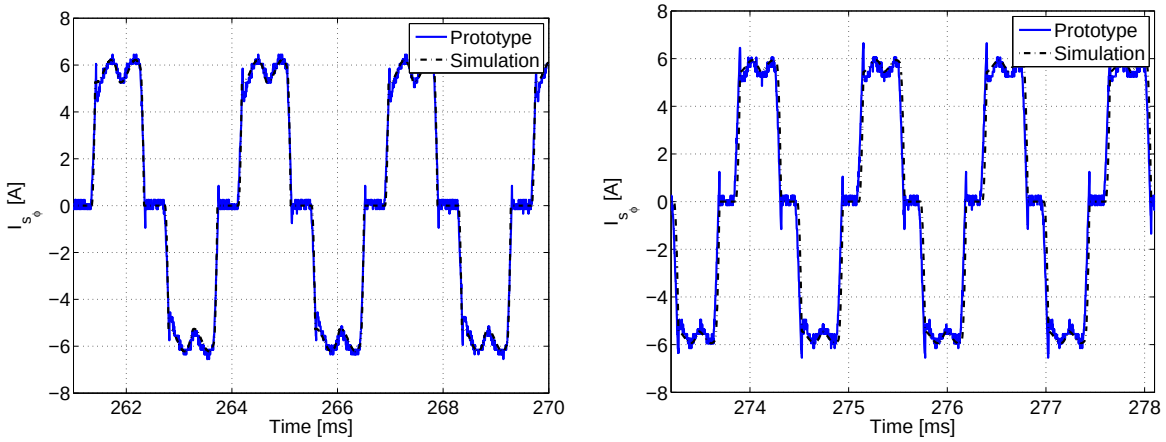

(a) $f = 360$ Hz (b) $f = 800$ Hz

Figure 45 – Source current - simulation and prototype values - $V_{s_\phi} = 118$ V.

The Figure 47 shows the simulation and experimental rectifier input voltage with $V_{s_\phi} = 118$ V. As can be seen the waveforms are very similar, which proves that the simulation, consequently the model, are in agreement with the experimental results. The notch effect is observed due to the input inductance.

As analyzed in the mathematical model, the notch effect causes a decrease in the output voltage. Table 25 shows the comparison between the simulated and experimental values. The values are close, which also validates the mathematical model. The

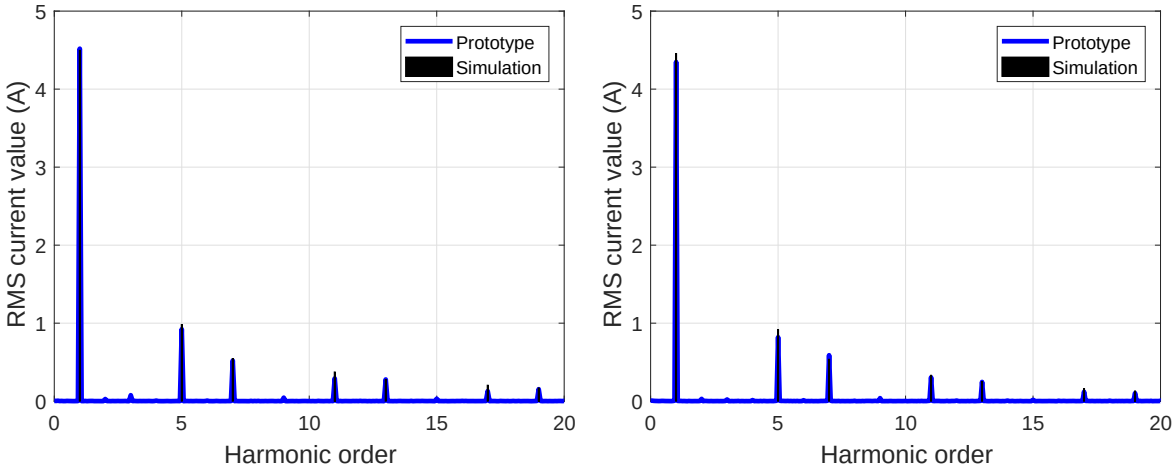

(a) $f = 360\,\text{Hz}$ (b) $f = 800\,\text{Hz}$

Figure 46 – Harmonic spectra of the source current - simulation and prototype values - $V_{s_\phi} = 118\,\text{V}$.

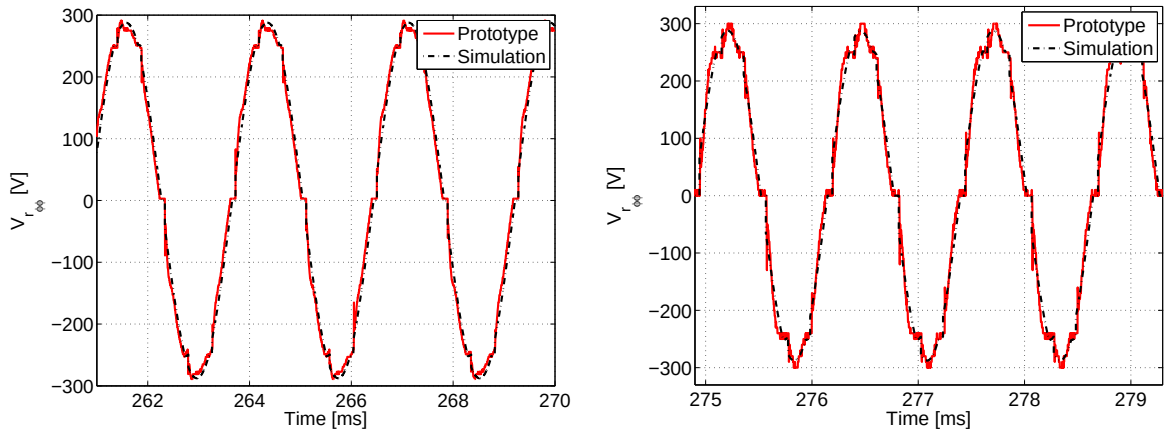

(a) $f = 360\,\text{Hz}$ (b) $f = 800\,\text{Hz}$

Figure 47 – Voltage at the input of the rectifier - simulation and prototype values - $V_{s_\phi} = 118\,\text{V}$.

difference occurs because the losses and voltage drops present in the system are not included in the model. As expected, with increasing frequency, the value of $\overline{V_o}$ decreases, this occurs because of the notch effect that changes with frequency.

Table 25 – Comparison of the $\overline{V_o}$ value obtained by simulation and at the prototype with L filter.

$V_{s_\phi} = 108\,\text{V}$			$V_{s_\phi} = 118\,\text{V}$		
	Simulation (V)	Prototype (V)		Simulation (V)	Prototype (V)
360 Hz	251	242	360 Hz	274.3	264
800 Hz	249	236	800 Hz	272.3	258

3.2 Second order input LC filter

The prototype was assembled to verify the analysis performed previously (Figure 48). As done for the L filter, for the sake of simplicity, only one arm of the 12 pulse-rectifier was tested. With this configuration the 5^{th} and 7^{th} harmonics of the input current are not cancelated, but the behavior of the system is the same.

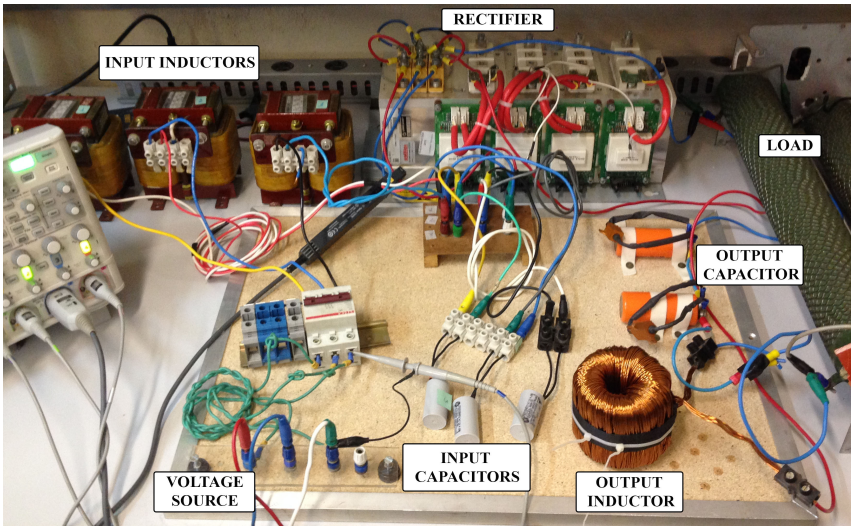

Figure 48 – Prototype with LC input filter.

The tests were done in a small scale for 360-800 Hz with the data present in Table 26. The input filter was designed according to the methodology presented in section 2.3.2. In order to compare with the previous analysis, the same cutoff frequency (1200 Hz) was chosen. The maximum allowed inductor value was found by equation (2.39) and for $P_o = 2.5\,\text{kW}$, $L_{in_{\phi max}}$ is around 3.8 mH. According to the availability in the laboratory it was chosen $L_{in_\phi} = 2.9\,\text{mH}$ and $C_{in_{\phi\phi}} = 2\,\mu\text{F}$.

The output filter values have been chosen to attenuate the harmonics in the DC side and according to the available components. In addition, the tests were performed with resistive load and not with constant power as the previous analysis. However, in order to have an adequate comparison parameter, the circuit was simulated with the experimental data (Table 26) at the PLECS software. The voltage source used is 4500iL AC Power Source - California Instruments and the diode bridge is the SKKD 46/12 from Semikron. The LC prototype was assembled in a different laboratory from the L prototype and, because of this, the power source and rectifier are of different models.

Figure 49 shows the voltage and current at the source with $V_{s_\phi} = 118\,\text{V}$ and Figure 50 shows the source current in the prototype and in the simulation. As can be seen, the waveforms are visually similar. Figure 51 shows the simulation and prototype harmonic spectra of i_{s_ϕ} and the harmonics values from the simulation and prototype are

Table 26 – Prototype parameters with LC input filter.

Variable	Symbol	Value
Supply rms phase voltage	V_{s_ϕ}	108 V and 118 V
Supply frequency	f	360 Hz and 800 Hz
Input filter inductor	L_{in_ϕ}	2.9 mH
Input filter capacitor (Δ connection)	$C_{in_{\phi\phi}}$	2 µF
Output resistor load	R_o	33.33 Ω
Output filter inductor	L_{out}	1 mH
Output filter capacitor	C_{out}	235 µF

very close. As expected, the 5$^{\text{th}}$ and 7$^{\text{th}}$ harmonics appear, since the transformer was not used. The higher frequency components were attenuated by the filter.

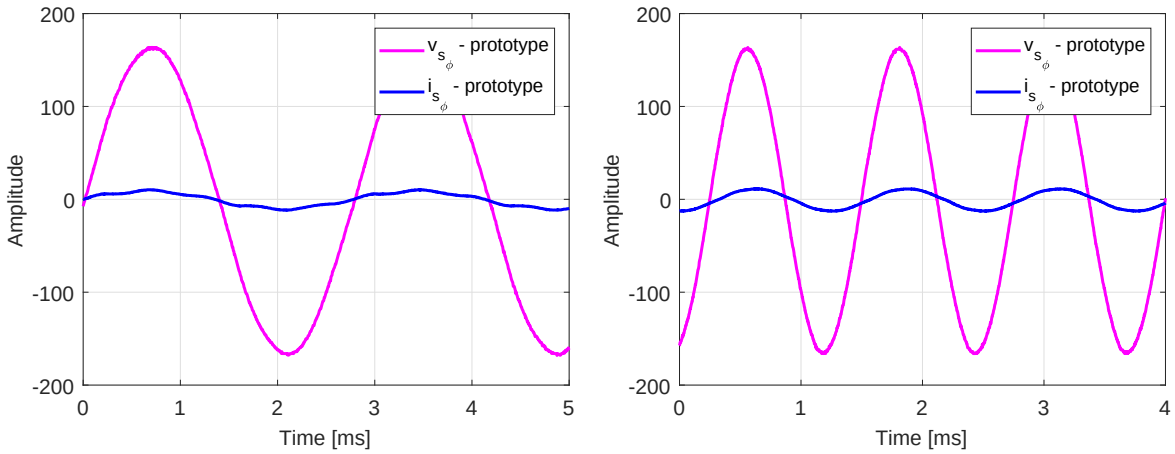

(a) $f = 360$ Hz (b) $f = 800$ Hz

Figure 49 – Voltage and current at the source - prototype values -$V_{s_\phi} = 118$ V.

The Figure 52 shows the output voltage waveforms with $V_{s_\phi} = 118$ V and Table 27 shows the comparison of the average value of $\overline{V_o}$ at the prototype and at the PLECS simulation. The values are very similar and the differences are due to the real conditions that are not considered in the simulation. As expected, the output voltage increase with increasing the frequency, with $V_{s_\phi} = 118$ V, for 360 Hz the relation $\overline{V_o}/V_{s_\phi} = 2.02$ and for 800 Hz $\overline{V_o}/V_{s_\phi} = 2.54$. This effect is due to resonance that was discussed in the previous sections.

To better understand the increase in the output voltage at 800 Hz, the voltage at the rectifier input must be analyzed. Figure 53 shows v_{r_ϕ} obtained by the prototype and by the simulation with $V_{s_\phi} = 118$ V. As can be seen, the waveforms are similar, in the prototype the peak values are attenuated. The waveforms at 360 Hz exhibit greater dis-

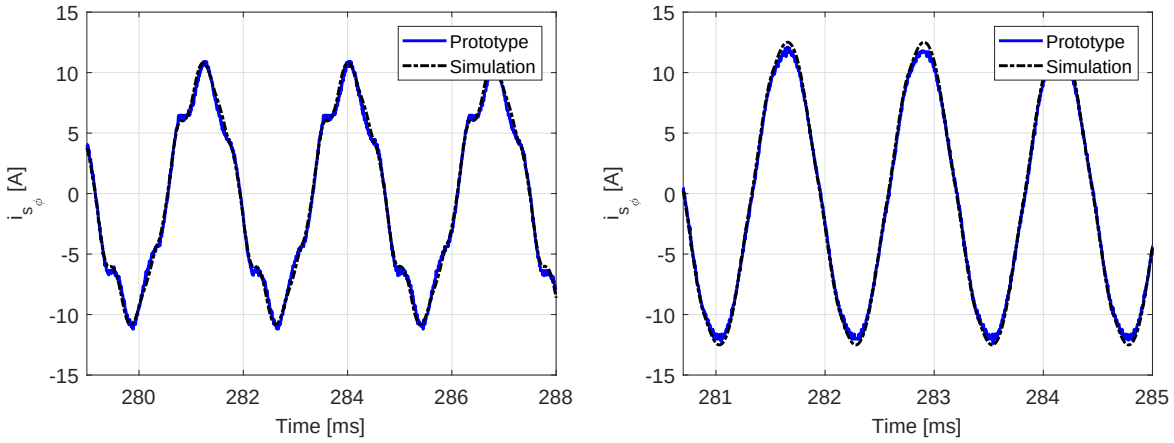

(a) $f = 360\,\text{Hz}$ (b) $f = 800\,\text{Hz}$

Figure 50 – Source current - simulation and prototype values -$V_{s_\phi} = 118\,\text{V}$.

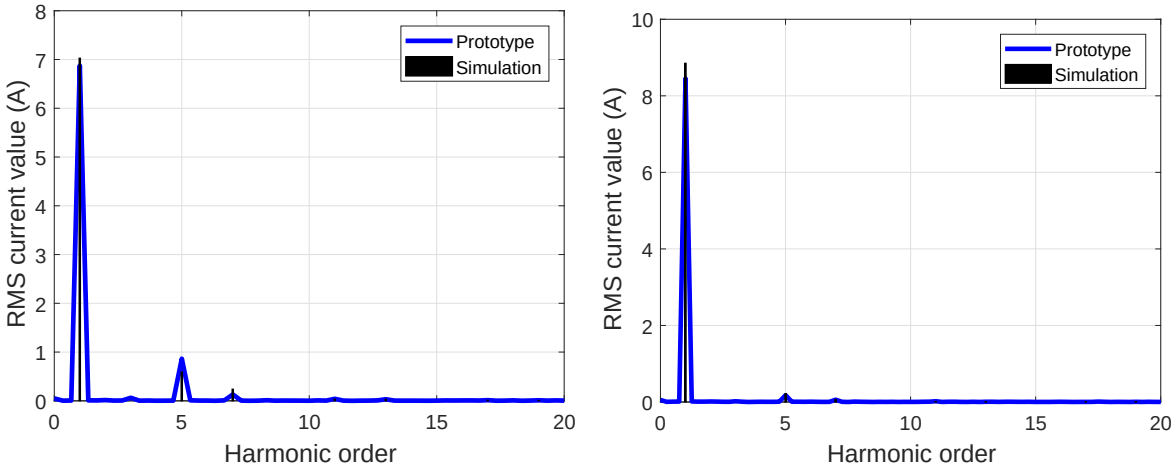

(a) $f = 360\,\text{Hz}$ (b) $f = 800\,\text{Hz}$

Figure 51 – Harmonic spectra of the source current - simulation and prototype values -$V_{s_\phi} = 118\,\text{V}$.

Table 27 – Comparison of the $\overline{V_o}$ value obtained by simulation and at the prototype.

$V_{s_\phi} = 108\,\text{V}$			$V_{s_\phi} = 118\,\text{V}$		
	Simulation (V)	Prototype (V)		Simulation (V)	Prototype (V)
360 Hz	263.8	258.4	360 Hz	288.1	283.1
800 Hz	280.2	273.4	800 Hz	306.2	299.5

tortion since the 5$^{\text{th}}$ and 7$^{\text{th}}$ harmonics are close to the filter cutoff frequency (1200 Hz), so they are amplified. Figure 54 shows the harmonic spectra of v_{r_ϕ} obtained by the prototype for 360 Hz and 800 Hz. As can been seen, at 800 Hz the fundamental value is amplified, since it is close to the filter resonance value (1200 Hz), which causes an increase in the output voltage ($\overline{V_o}$). For 360 Hz, the 5$^{\text{th}}$ harmonic is amplified, once it is close to 1200 Hz, making the voltage waveform more distorted.

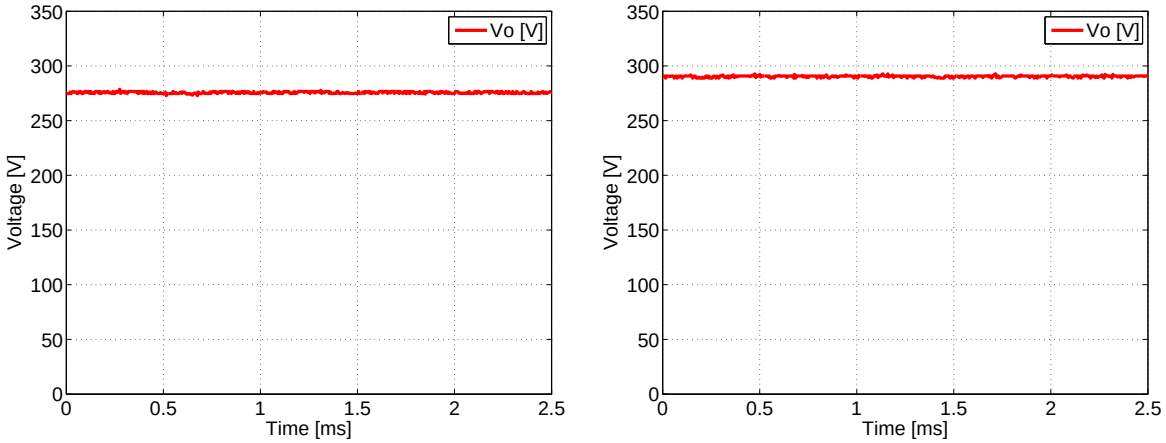

(a) $f = 360\,\text{Hz}$ (b) $f = 800\,\text{Hz}$

Figure 52 – Experimental results of the output voltage with LC filter - $V_{s_\phi} = 118\,\text{V}$.

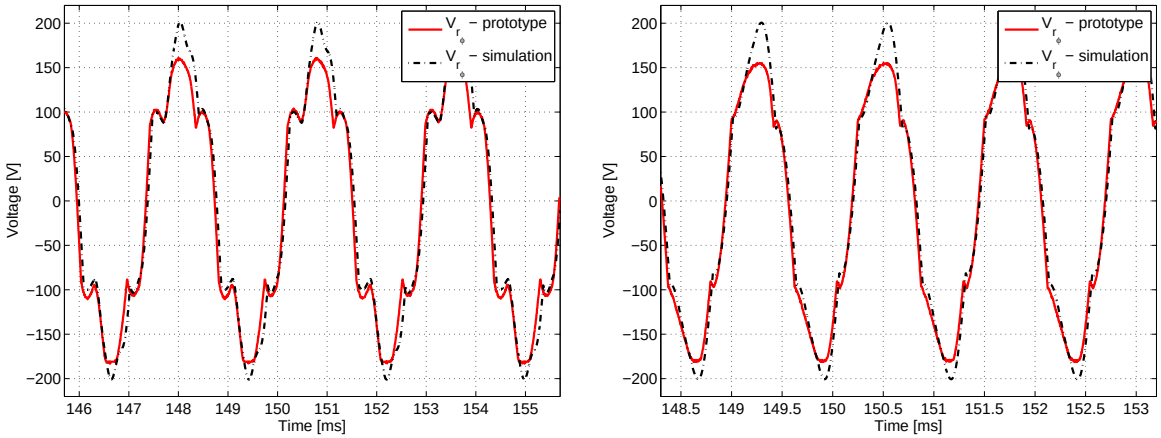

(a) $f = 360\,\text{Hz}$ (b) $f = 800\,\text{Hz}$

Figure 53 – Voltage at the input of the rectifier - simulation and prototype values -$V_{s_\phi} = 118\,\text{V}$.

3.3 Conclusion

In this chapter the experimental results of the circuit were shown.The purpose of this analysis was to validate the mathematical model together with the simulation.

The prototype was done in small scale following the same design method developed previously. The rectifier was assembled with L filter and LC filter. In order to compare the results, simulations were performed with the prototype data. All the results are in agreement and are coherent, which shows that the mathematical model is robust and its use is valid.

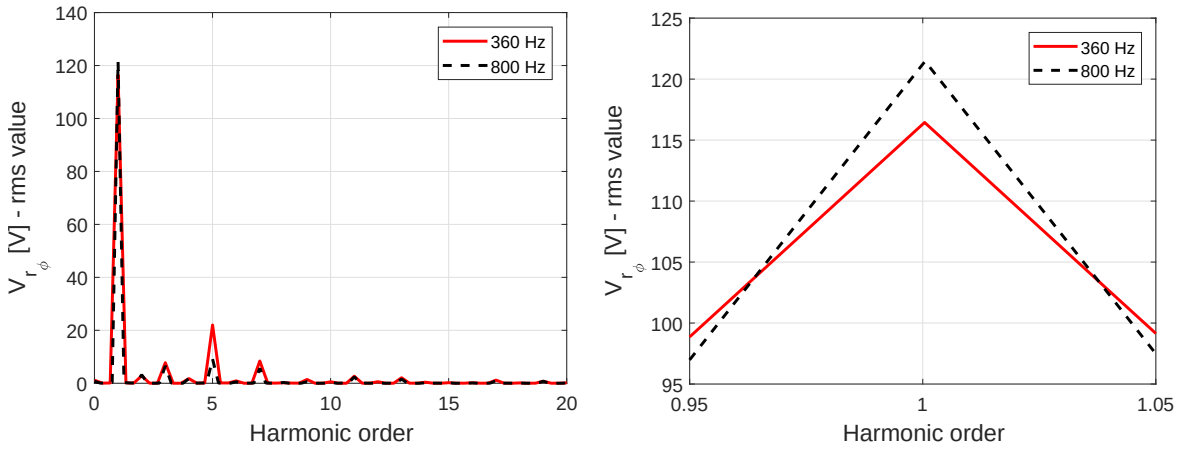

(a) (b) Zoom at the fundamental.

Figure 54 – Harmonic spectra of the voltage at the input of the rectifier - prototype values -$V_{s_\phi} = 118\,\mathrm{V}$.

4 24 pulse rectifier

4.1 Introduction

In this chapter, it will be investigate the use the 24-pulse rectifier (Figure 55). There are some ways to build the transformer of this rectifier (PANCHBHAI *et al.*, 2016; SINGH *et al.*, 2006; NESAN; J.JEGADHISH, 2015; KIRAN L PHANI KUMAR; VEERANJANEYULU, 2015). The important is that the currents in the secondaries of the transformer have a phase displacement of 15°. With a balanced load, the cancellation of some harmonics of the input current occurs, leaving only the harmonics above the 23th. It was used an primary in Y with four secondaries: Y, Delta, Zig-zag (+15) and Zig-zag (-15). An DC filter was design in order to limit the output voltage ripple as explained in section 2.1.

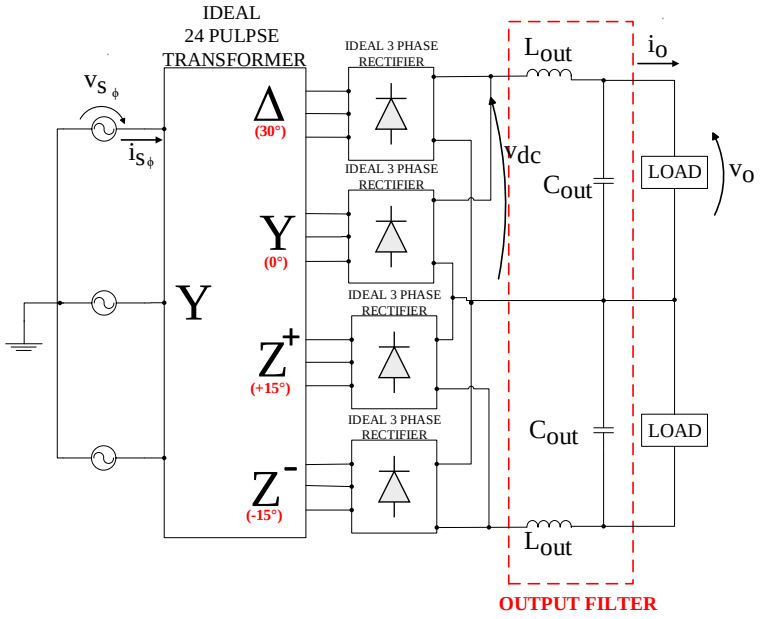

Figure 55 – Topology of a passive three-phase 24-pulse rectifier.

Figure 56 shows the voltage and current at the source with the data of Table 28. Figure 57 and Table 29 show the input current harmonic spectra. Due to the transformer, the input current has 12 levels. As can be seen, the harmonics before the 23th are eliminated in the primary side. Although, the high order harmonics are outside the standards limits. Therefore, it is necessary to study of an input filter. The output voltage and current are shown in Figure 58 and, as can be seen, the voltage ripple is within the limits establish by the standard.

Table 28 – Simulation parameters - 24 pulse rectifier.

Variable	Symbol	Value
Supply rms phase voltage	V_{s_ϕ}	118 V
Supply frequency	f	360 Hz
Power in each rectifier	$P_{3\phi}$	25 kW
Voltage ratio	N	1
Output filter inductor	L_{out}	500 mH
Output filter capacitor	C_{out}	203 µF

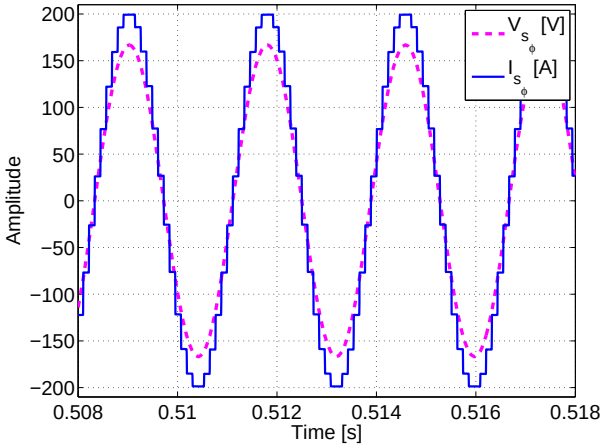

Figure 56 – Input voltage (magenta) and current (blue) with an LC DC filter - $V_{s_\phi} = 118$ V and $f = 360$ Hz.

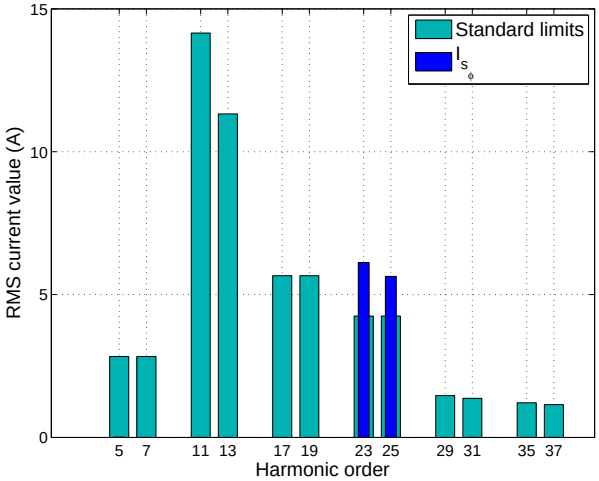

Figure 57 – Harmonic content of the input current with LC DC filter - $V_{s_\phi} = 118$ V and $f = 360$ Hz.

Table 29 – Numeric values of the Figure 57 - Harmonic content of the input current with LC DC filter - $V_{s_\phi} = 118$ V and $f = 360$ Hz.

Harmonic order	I_{s_ϕ} (A)
23	6.12
25	5.64

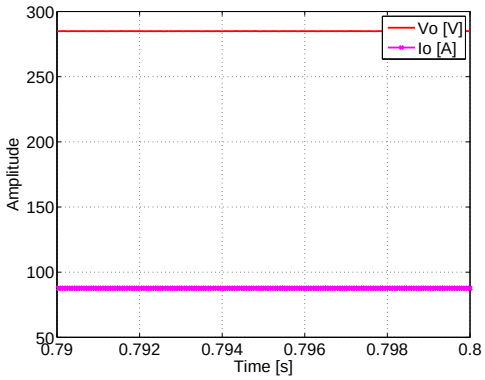

Figure 58 – Output voltage (red) and current (green) with an LC DC filter - $V_{s_\phi} = 118$ V and $f = 360$ Hz.

4.2 First order L filter

The analyzes of the 24-pulse is very similar with the 12-pulse rectifier, once the model was developed based on the 6-pulse rectifier. The harmonic content of the 24-pulse rectifier is lower than in the 12-pulse rectifier, so the value of $L_{in_{\phi_{min}}}$ is not a issue for this topology. However, the decrease in the output voltage due to the notch effect happens in the same way. The current values that flows through the input inductors in the 24-pulse rectifier are the same as in the case of the 12-pulse. The output voltage at each load is a combination of two 6-pulse rectifiers once they are connected in parallel and, since the average values are the same, the average load voltage is the same as in only one 6-pulse rectifier. Therefore, the equation developed in the 12-pulse case is a good approximation for the 24-pulse case. Using equation (2.2), that is rewritten on equation (4.1), it is possible to find the maximum inductance value to produce the minimum allowed output voltage (250 V).Using the maximum N value allowed: 1.0144 (section 2.2.1), $P_{3\phi} = 25$ kW and with the worst operation condition: $f = 800$ Hz and $V_{s_\phi} = 108$ V, it is found $L_{in_{\phi_{max}}} = 13.05$ µH. This value is the same as for the 12-pulse rectifier.

$$\overline{V_o} P_{3\phi} - \frac{3\sqrt{6}}{\pi} V_{s_\phi} N P_{3\phi} + 6 f L_{in_\phi} \overline{V_o} 5 = 0 \tag{4.1}$$

With this operation condition, the circuit was simulated in the software PLECS. Figure 59 shows the output voltage and the average value is 252.8 V, which is really close

to the expected according to the mathematical model. Figure 60, 61 and Table 30show the waveform and harmonic spectra of the input current, respectively. As can be seen, the harmonic content complies with the standard limits and the harmonics before the 23$^{\text{th}}$ are eliminated.

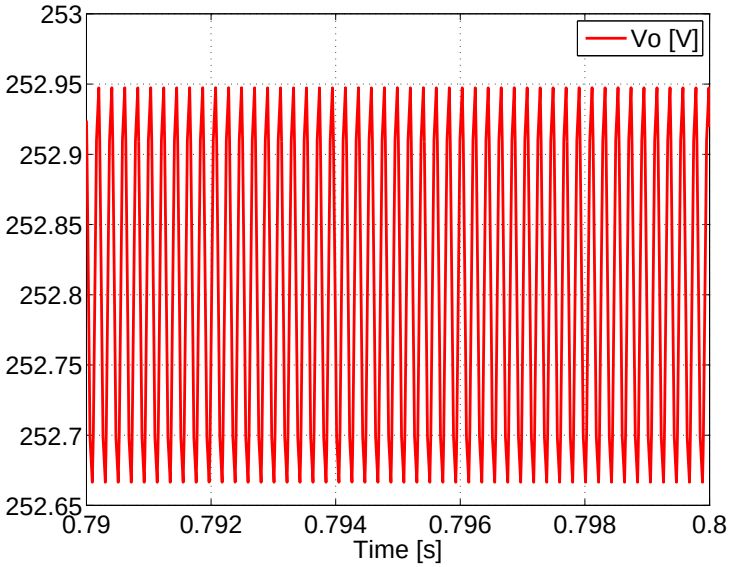

Figure 59 – 24-pulse rectifier - voltage at the load with $f = 800\,\text{Hz}$ and $V_{s_\phi} = 108\,\text{V}$.

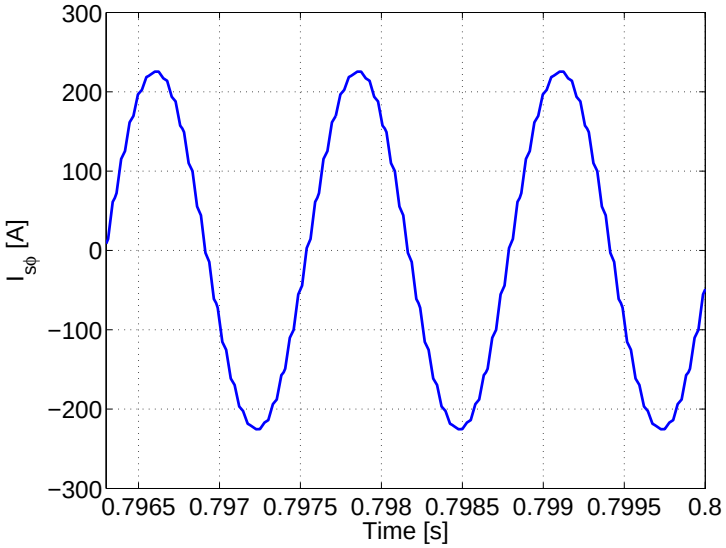

Figure 60 – 24-pulse rectifier - source current with $f = 800\,\text{Hz}$ and $V_{s_\phi} = 108\,\text{V}$.

As happened in the 12 pulse rectifier, this inductance value is too small to be used in the real circuits when compared with the data provided by (GONG *et al.*, 2003; MINO *et al.*, 2005; GONG *et al.*, 2005; BAGHRAMIAN *et al.*, 2011; CHIVITE-ZABALZA; FORSYTH, 2005; CROSS *et al.*, 2009). In the simulation, the losses, the inductances of transformers, wires and generator and the diodes voltage drops are not been considered. Therefore it is necessary to explore other solutions.

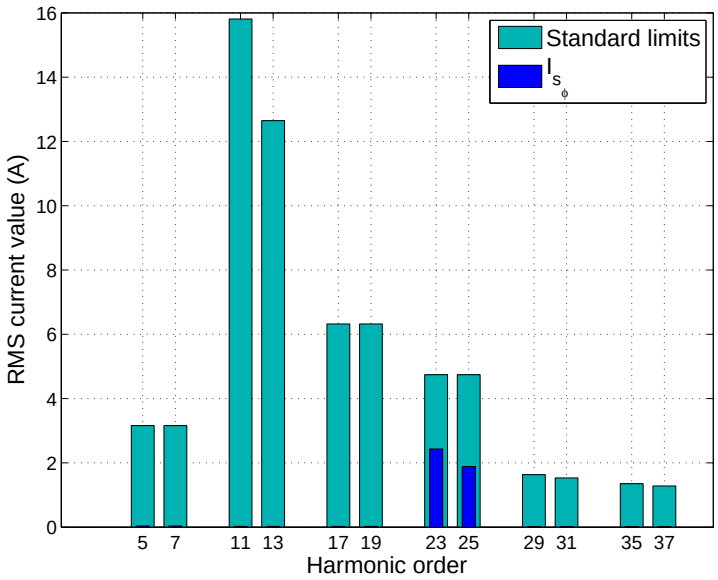

Figure 61 – 24-pulse rectifier - current spectra of current in the source (dark blue) and the standard limits (light blue) with $f = 800\,\text{Hz}$ and $V_{s_\phi} = 108\,\text{V}$.

Table 30 – Numeric values of the Figure 61 - 24-pulse rectifier - current spectra of current in the source (dark blue) and the standard limits (light blue) with $f = 800\,\text{Hz}$ and $V_{s_\phi} = 108\,\text{V}$.

Harmonic order	I_{s_ϕ} (A)
23	2.23
25	1.97

4.3 Second order LC filter

The analysis of the second order filter at the 24-pulse rectifier is the same showed at the section 2.3, once the filter design was performed for each 6-pulse rectifier, and the characteristics in this part of the circuit are the same, independent of the rectifier pulse number. Therefore, $L_{in_\phi} = 250.6\,\mu\text{H}$ and $C_{in_{\phi\phi}} = 23.39\,\mu\text{F}$. The circuit was simulated at the software PLECS with the data present in Table 31.

Table 31 – PLECS simulation parameters - LC filter with variable frequency.

Variable	Symbol	Value
Output power in each rectifier	P_o	25 kW
Supply rms phase voltage	V_{s_ϕ}	108 V and 118 V
Voltage ratio	N	1
Input filter inductor	L_{in_ϕ}	250.6 µH
Input filter capacitor (Δ connection)	$C_{in_{\phi\phi}}$	23.39 µF
Output filter inductor	L_{out}	500 µH
Output filter capacitor	C_{out}	203 µF

Figure 62 shows the output voltage for both frequencies, the average voltage for 360 Hz is 309.1 V and for 800 Hz is 453.3 V. These values are the same as in the analysis at section 2.3.4.2, once for the 24-pulse rectifier the load does not feel the difference. The output voltage increases significantly, this happens due to the resonance effect that occurs. The explanation for this phenomenon can be found in section 2.3.4.2.

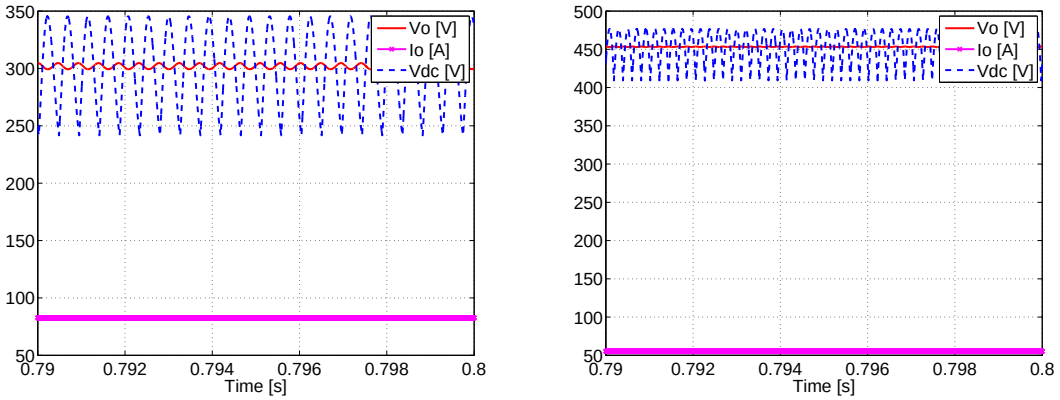

(a) $f = 360\,\text{Hz}$ (b) $f = 800\,\text{Hz}$

Figure 62 – Voltage at the output of the rectifiers (blue), load current (magenta) and load voltage (red) with $V_{s_\phi} = 118\,\text{V}$.

As occurs in the 12-pulse rectifier, because of the resonance phenomenon, the output voltage goes beyond the limits allowed by the standard, and it is not possible to use this configuration for the analyzed case.

4.4 Conclusion

As shown in this chapter, even increasing the levels of the rectifier, it is not possible to meet the aeronautical standards with respect to the input current and the output voltage simultaneously. This is because the basic structure is the same. The analyses and phenomena that occur are the same as those described in previous chapters.

With the L filter, the output voltage decreases due to the notch effect and, with the LC filter, the resonance effect is observed and the output voltage increases beyond the allowed by the standard.

Conclusion and future works

The modern airplanes operate with a variable frequency (360 - 800 Hz) and due to increased power demand, the systems tend to use high voltage dc buses (± 270V). Considering this scenario, this work analyzed the feasibility of using a passive rectifier to be applied in aeronautical systems. Firstly, a complete analysis of the 12-pulse rectifier for 50 kW was made with two sorts of input filters: L and LC. In a second analysis, a simplified analysis of the 24-pulse rectifier was performed, also with two types of input filter: L and LC.

For the 12 pulse-rectifier with a L input filter, the mathematical model, simulation and prototype were performed. All results are in agreement, which shows that the mathematical model is robust and its use is valid.

The circuit was analyzed in two situations: fixed frequency (400 Hz) and variable frequency (360 - 800 Hz). The results for both situations are similar. Using a unitary transformer voltage ratio it is not possible to comply with the aeronautical standards in respect to the input current harmonic content and the output voltage simultaneously. Changing the voltage ratio to its maximum value (1.0144) it is possible to find an inductance value that satisfies both cases, but this value is too small compared to the typical circuit values (inductances of transformers, wires and generator). For that reason, this solution becomes impractical.

The 12-pulse rectifier with input LC filter was analyzed with fixed and variable frequency scenarios. The aim is to comply with aeronautical standards with respect to the harmonic content of the input current and the limits of the output voltage. A mathematical model and a method for designing the input filter were developed. The leakage inductance of the transformer and generator must be considered, as well the cables inductances. The use of the LC filter after the transformer (secondary side) allows to include such inductances on L_{in_ϕ}. If the filter was used at the transformer primary side, its leakage inductance would affect the system behavior similarly to the L filter analysis.

In the filter design, the cutoff frequency should be greater than the maximum operating frequency and lower than the lowest harmonic liable to exist in the circuit. Moreover, there is a maximum value of L_{in_ϕ} so that the nominal power can be delivered to the load.

For the circuit operating at fixed frequency it is possible to find a value for the LC filter compatible with the real circuit values. The harmonic limits of the input current are met and, considering that the real circuit presents losses, the output voltage

also meets aeronautical standards.

With the circuit operating with variable frequency, although it is possible to attenuate the harmonic components, the allowed range for the filter cutoff frequency is very narrow and the resonance phenomenon occurs, increasing the output voltage. Therefore, it is not possible to meet the requirements of aeronautical standards.

Therefore, it is concluded that the solution with the 12-pulse rectifier with LC input filter, in the conditions analyzed, is feasible for a system operating at fixed frequency, although for variable frequency situation it is not possible to comply with the output voltage standards limits. The use of high-order filter would increase the complexity of the system, making it difficult to be use.

A low-scale prototype was implemented to validate the analysis of the 12-pulse rectifier with the two input filters: L and LC. The effect of the output voltage and the current source were analyzed. The experimental results are in agreement with the simulated and, consequently, with the model.

It was also analyzed the 24-pulse rectifier. The objective is to analyze if increasing the number of rectifier pulse it is possible to solve the issue and meet the standard constraints. It has been shown that increasing the number of pulses makes no difference in the analysis, once the filter design is performed for each 6-pulse rectifier, and the characteristics are the same, independent of the rectifier pulse number. As happens in the 12-pulse rectifier, with the L filter, the effect of the notch occurs which leads to a decrease in the output voltage and with the LC resonance occurs raising the output voltage.

A possible solution to this problem is use active rectifiers, such as Vienna rectifier. This rectifier allows a better control of the input current and the output voltage, moreover, allows the implementation of symmetric DC buses without the need of na additional circuit. Finally, it is suggested as future work the investigation of active rectifiers that can be applied to aeronautical systems and meet the standards constraints.

Bibliography

BAGHRAMIAN, A.; CROSS, A.; FORSYTH, A. Interactions within heterogeneous systems of uncontrolled rectifiers for aircraft electrical power systems. *IET Electrical Systems in Transportation*, v. 1, n. 1, p. 49–60, March 2011. ISSN 2042-9738. Citado 5 vezes nas páginas 38, 41, 45, 46, and 73.

CHIVITE-ZABALZA, F. J.; FORSYTH, A. J. A simple, passive 24-pulse ac-dc converter with inherent load balancing using harmonic voltage injection. In: *2005 IEEE 36th Power Electronics Specialists Conference*. [S.l.: s.n.], 2005. p. 76–82. ISSN 0275-9306. Citado 5 vezes nas páginas 38, 41, 45, 46, and 73.

CLOSE, C. *The analysis of linear circuits*. Harcourt, Brace & World, 1966. (Harbrace series in electrical engineering). Disponível em: <https://books.google.co.uk/books?id=xeZSAAAAMAAJ>. Citado 2 vezes nas páginas 46 and 47.

CROSS, A.; BAGHRAMIAN, A.; FORSYTH, A. Approximate, average, dynamic models of uncontrolled rectifiers for aircraft applications. *IET Power Electronics*, v. 2, n. 4, p. 398–409, July 2009. ISSN 1755-4535. Citado 6 vezes nas páginas 26, 38, 41, 45, 46, and 73.

EMADI, K.; EHSANI, M. Aircraft power systems: technology, state of the art, and future trends. *IEEE Aerospace and Electronic Systems Magazine*, v. 15, n. 1, p. 28–32, Jan 2000. ISSN 0885-8985. Citado na página 21.

FADIL A.E., M. A. S. R. A. Electrical distribution power systems of modern civil aircrafts. In: *2nd International Conference on Energy Systems and Technologies*. [S.l.: s.n.], 2013. Citado na página 21.

GONG, G.; DROFENIK, U.; KOLAR, J. W. 12-pulse rectifier for more electric aircraft applications. In: *IEEE International Conference on Industrial Technology, 2003*. [S.l.: s.n.], 2003. v. 2, p. 1096–1101 Vol.2. Citado 9 vezes nas páginas 10, 24, 25, 26, 38, 41, 45, 46, and 73.

GONG, G.; HELDWEIN, M. L.; DROFENIK, U.; MINO, K.; KOLAR, J. W. Comparative evaluation of three-phase high power factor ac-dc converter concepts for application in future more electric aircrafts. In: *Applied Power Electronics Conference and Exposition, 2004. APEC '04. Nineteenth Annual IEEE*. [S.l.: s.n.], 2004. v. 2, p. 1152–1159 vol.2. Citado 3 vezes nas páginas 10, 25, and 26.

GONG, G.; HELDWEIN, M. L.; DROFENIK, U.; MINIBOCK, J.; MINO, K.; KOLAR, J. W. Comparative evaluation of three-phase high-power-factor ac-dc converter concepts for application in future more electric aircraft. *IEEE Transactions on Industrial Electronics*, v. 52, n. 3, p. 727–737, June 2005. ISSN 0278-0046. Citado 8 vezes nas páginas 10, 25, 26, 38, 41, 45, 46, and 73.

GUERREIRO, J. F.; POMILIO, J. A.; BUSARELLO, T. D. C. Design and implementation of a multilevel active power filter for more electric aircraft variable frequency systems. In: *2013 Brazilian Power Electronics Conference*. [S.l.: s.n.], 2013. p. 1001–1007. ISSN 2165-0454. Citado na página 60.

JIANG, L.; CHEN, Q.; MAO, L.; REN, X.; RUAN, X. Asymmetrical operation analysis of multi-pulse atru. In: *Proceedings of The 7th International Power Electronics and Motion Control Conference*. [S.l.: s.n.], 2012. v. 1, p. 660–665. Citado na página 24.

KARIMI, K. J.; MONG, A. C. Modeling nonlinear loads for aerospace power systems. In: *Energy Conversion Engineering Conference, 2002. IECEC '02. 2002 37th Intersociety*. [S.l.: s.n.], 2002. p. 33–38. Citado na página 24.

KIRAN L PHANI KUMAR, N. S. R. M.; VEERANJANEYULU, P. Design and analysis of a 24-pulse ac-dc power converter by employing a pulse doubling technique for asynchronous drive. *International Journal of Conceptions on Electrical and Electronics Engineering*, v. 3, n. 1, p. 8–12, April 2015. ISSN 2345-9603. Citado na página 70.

MINO, K.; GONG, G.; KOLAR, J. W. Novel hybrid 12-pulse boost-type rectifier with controlled output voltage. *IEEE Transactions on Aerospace and Electronic Systems*, v. 41, n. 3, p. 1008–1018, July 2005. ISSN 0018-9251. Citado 9 vezes nas páginas 10, 24, 25, 26, 38, 41, 45, 46, and 73.

MOHAN, N.; UNDELAND, T. M.; ROBBINS, W. P. *Power Electronics. Converters, Applications and Design*. third. [S.l.]: John Wiley and Sons, Inc, 2003. Citado na página 62.

MONROY, A. O.; LE-HUY, H.; LAVOIE, C. Modeling and simulation of a 24-pulse transformer rectifier unit for more electric aircraft power system. In: *2012 Electrical Systems for Aircraft, Railway and Ship Propulsion*. [S.l.: s.n.], 2012. p. 1–5. ISSN 2165-9400. Citado na página 24.

NESAN, R.; J.JEGADHISH. Designing and harmonic analysis of a new 24-pulse rectifier using diodes with phase shifting transformer. *International Journal of Science, Engineering and Technology Research (IJSETR)*, v. 4, n. 2, p. 273–276, February 2015. ISSN 2278–7798. Citado na página 70.

NYA, B. H.; BROMBACH, J.; SCHULZ, D. Benefits of higher voltage levels in aircraft electrical power systems. In: *2012 Electrical Systems for Aircraft, Railway and Ship Propulsion*. [S.l.: s.n.], 2012. p. 1–5. ISSN 2165-9400. Citado na página 21.

PANCHBHAI, A.; SHAH, H.; NIZAMI, N. Line regulation in 24 pulse controlled rectifier. In: *2016 IEEE 6th International Conference on Power Systems (ICPS)*. [S.l.: s.n.], 2016. p. 1–6. Citado na página 70.

RASHID, M. *Eletrônica de potência: circuitos, dispositivos e aplicações*. Makron, 1999. ISBN 9788534605984. Disponível em: <https://books.google.com.br/books?id=n9tIAAAACAAJ>. Citado na página 31.

ROSERO, J. A.; ORTEGA, J. A.; ALDABAS, E.; ROMERAL, L. Moving towards a more electric aircraft. *IEEE Aerospace and Electronic Systems Magazine*, v. 22, n. 3, p. 3–9, March 2007. ISSN 0885-8985. Citado na página 21.

SARLIOGLU, B.; MORRIS, C. T. More electric aircraft: Review, challenges, and opportunities for commercial transport aircraft. *IEEE Transactions on Transportation Electrification*, v. 1, n. 1, p. 54–64, June 2015. Citado na página 21.

SILVA, M.; HENSGENS, N.; OLIVER, J.; ALOU, P.; GARCíA, .; COBOS, J. A. Isolated swiss-forward three-phase rectifier for aircraft applications. In: *2014 IEEE Applied Power Electronics Conference and Exposition - APEC 2014*. [S.l.: s.n.], 2014. p. 951–958. ISSN 1048-2334. Citado na página 24.

SINGH, B.; BHUVANESWARI, G.; GARG, V. T-connected autotransformer-based 24-pulse ac-dc converter for variable frequency induction motor drives. *IEEE Transactions on Energy Conversion*, v. 21, n. 3, p. 663–672, Sept 2006. ISSN 0885-8969. Citado na página 70.

STATES, U. Book, Online. *RTCA Inc Document RTCA DO-160E - Environmental conditions and test procedures for airborne equipment*. [S.l.]: U.S. Dept. of Transportation, Federal Aviation Administration [Washington, D.C.], 2007. 2 p. : p. Citado na página 21.

STATES, U. Book. *Aircraft Electric Power Characteristics - MIL-STD-704F*. [S.l.]: Departmente of Defense - United States of America, 2008. 1-40 p. Citado na página 21.

VITOI, L. A.; POMILIO, J. A.; BRANDAO, D. I. Analysis of 12-pulse diode rectifier operating in aircraft systems with constant frequency. In: *14th Brazilian Power Electronics Conference, COBEP 2017*. [S.l.: s.n.], 2017. Citado na página 26.

VITOI, L. A.; POMILIO, J. A.; BRANDAO, D. I. Analysis of 12-pulse diode rectifier operating in aircraft systems with variable frequency. In: *3rd IEEE Southern Power Electronics Conference, SPEC 2017*. [S.l.: s.n.], 2017. Citado na página 26.

WHEELER, P.; BOZHKO, S. The more electric aircraft: Technology and challenges. *IEEE Electrification Magazine*, v. 2, n. 4, p. 6–12, Dec 2014. ISSN 2325-5897. Citado na página 21.

Appendix

APPENDIX A – Calculation of the possible values of Z_1 (R_1 and X_1)

As can be seen in section 2.3.2, for the calculation of V_o it is necessary to find the value of R_1, which is found only by simulation.This appendix aims to advance a little in the calculation of R_1, determining the possible values it can assume.

The Figure 63 shows the equivalent Thevenin circuit seen by the rectifier at the fundamental frequency. The values of the Thevenin voltage ($V_{th_{\phi-1}}$) and impedance ($X_{th_{\phi-1}}$) are calculated by (2.33) and (2.34).

As shown in the simulation results (section 2.3.4.2 - Table 21), the load cannot be modeled as a pure resistance, it must contain a reactive part. Thus, the equivalent circuit per phase at the fundamental frequency must be modeled as shown in Figure 64. R_1 and X_1 compose the equivalent impedance seen by the filter at the fundamental frequency.

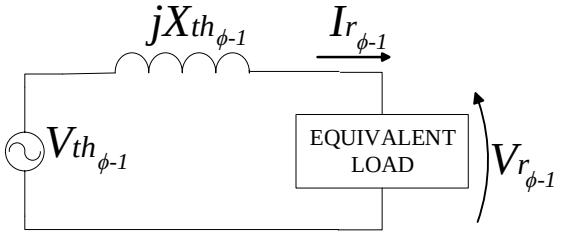

Figure 63 – Equivalent Thevenin circuit of LC input filter.

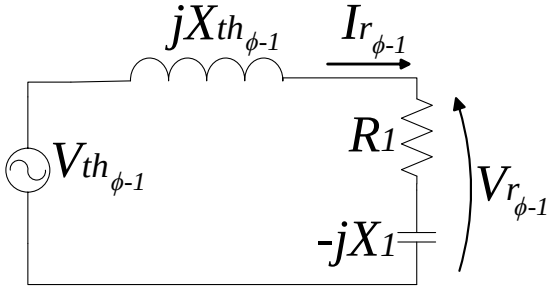

Figure 64 – Equivalent circuit per phase in the fundamental frequency.

As $V_{th_{\phi-1}}$ is purely sinusoidal, the entire active power is present at the funda-

mental frequency, thus (A.1) is valid.

$$P_{1\phi} = R_1 I_{r_{\phi-1}}^2 \tag{A.1}$$

Where

$$I_{r_{\phi-1}} = \frac{V_{th_{\phi-1}}}{\sqrt{R_1^2 + (X_{th_{\phi-1}} - X_1)^2}} \tag{A.2}$$

Substituting (A.2) in (A.1) results in equation (A.3) and its solution is given by (A.4).

$$R_1^2(P_{1\phi}) + R_1(-V_{th_{\phi-1}}^2) + P_{1\phi}(X_{th_{\phi-1}} - X_1)^2 = 0 \tag{A.3}$$

$$R_1 = \frac{V_{th_{\phi-1}}^2 \pm \sqrt{\Delta}}{2P_{1\phi}} \tag{A.4}$$

Where

$$\Delta = X_1^2(-4P_{1\phi}^2) + X_1(8X_{th_{\phi-1}}P_{1\phi}^2) + V_{th_{\phi-1}}^4 - 4P_{1\phi}^2 X_{th_{\phi-1}}^2 \tag{A.5}$$

This is a mathematical model, hence the real limitations must be considered.

- $V_{th_{\phi-1}}^2 \pm \sqrt{\Delta}$ must be greater than zero. It's clear that R_1 never assumes negative values.
- For R_1 to only assume real values, $\Delta > 0$, graphically it can be represented as the grey area in Figure 65.

With the simulation values used in section 2.3.4.2, which are shown in Table 32 and using equation (A.3), it is plotted the graph of $R_1 x X_1$ (Figure 66) and $R_1 x X_{eq}$ ($X_{eq} = X_{th_{\phi-1}} - X_1$) (Figure 67). As can be seen, these are the possible values of R_1 an X_1 for a fixed power (25 kW), the specific point where the circuit will be operating depends on the load on the DC side. Table 33 explicits the maximum and minimum values that X_1 and R_1 can assume.

Analyzing the Δ graph it can be seen that for a single Δ value there are two possible values of R_1 and X_1. Considering that the phase between the voltage and current at the rectifier input is not very large, there are two operating points. This characteristic is observed in the simulations: for a specific power there are two possible operating points.

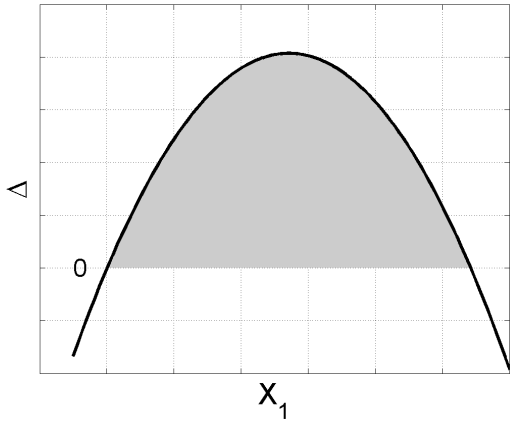

Figure 65 – Δ graph – the grey area indicates where R_1 only assumes real values.

Table 32 – PLECS simulation parameters - LC filter with variable frequency.

Variable	Symbol	Value
Output power in each rectifier	P_o	25 kW
Supply rms phase voltage	V_{s_ϕ}	118 V
Voltage ratio	N	1
Input filter inductor	L_{in_ϕ}	250.6 µH
Input filter capacitor (Δ connection)	$C_{in_{\phi\phi}}$	23.39 µF
Output filter inductor	L_{out}	500 µH
Output filter capacitor	C_{out}	200 µF

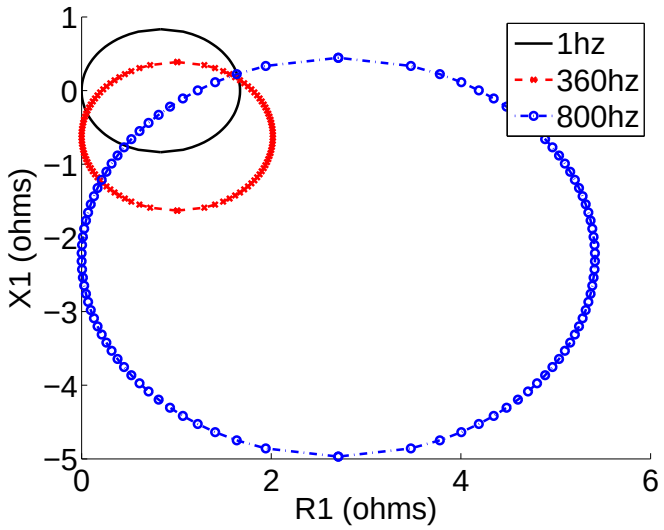

Figure 66 – Plot of the possible values of X_1 and R_1 in multiple frequencies.

In the analyzes carried out during the text, it was considered only the operating points with higher R_1 value, and hence larger load resistors (R_o). It was adopted this way, since in the real circuits the tendency is to start with an open circuit ($R_o \to \infty$) and decrease until reach the desired operating point. However, for the same power, there are

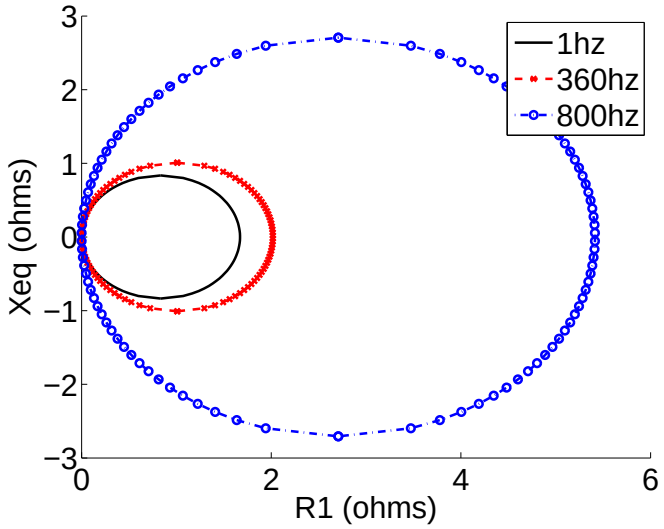

Figure 67 – Plot of the possible values of X_{eq} and R_1 in multiple frequencies.

Table 33 – Maximum and minimum values that X_1 and R_1 can assume.

	R_1	X_1
Minimum value	$\lim R_1 \to 0$	$X_{th_{\phi-1}} - V^2_{th_{\phi-1}}/(2P_{1\phi})$
Maximum value	$V^2_{th_{\phi-1}}/P_{1\phi}$	$X_{th_{\phi-1}} + V^2_{th_{\phi-1}}/(2P_{1\phi})$

two possible operating points.

To exemplify this characteristic, it was simulate the circuit with the data of Table 32 for the two operating points. Table 34 summarizes the results found for both cases.

Table 34 – Circuit operation points - $V_{s_\phi} = 118\,\text{V}$.

	$f = 360\,\text{Hz}$		$f = 800\,\text{Hz}$	
	Operating point 1	Operating point 2	Operating point 1	Operating point 2
P_o	25 kW	25 kW	25 kW	25 kW
R_o	3.65 Ω	0.3 Ω	8.22 Ω	1.67 Ω
V_o	301.93 V	86.45 V	453.3 V	204.37 V
R_1	2.01 Ω	0.18 Ω	4.51 Ω	0.92 Ω
X_1	−0.59 Ω	−0.04 Ω	−0.26 Ω	−0.23 Ω
$V_{r_{\phi-1}}$	135.06 $\angle -17.2$V	39.9 $\angle -85.7$V	194.15 $\angle -27.2$V	90.24 $\angle -79.7$V
$I_{r_{\phi-1}}$	64.23 $\angle -0.9$A	213.72 $\angle -72.6$A	42.99 $\angle -23.9$A	0.947 $\angle -14.1$A

In this way, the question is to know which are the operating points of the simulation. On the Figure 68 the black dots represent the values of the simulations and, as can be seen, they are contained in the calculated values. For the circuit tending to a

very low frequency ($f = 1$ Hz) it is possible to calculate this point, once its operating point tends toward a purely resistive impedance, which can be calculated by the equation (A.6).

$$R_1 = \frac{V_{th_{\phi-1}}^2}{P_{1\phi}} \tag{A.6}$$

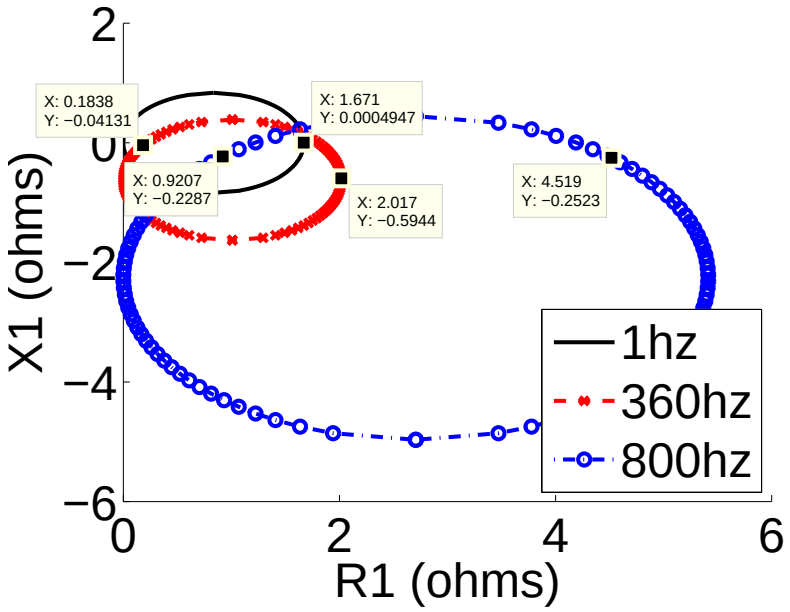

Figure 68 – Plot of the possible values of X_1 and R_1 and the simulation points (square markers).

With this mathematical model it is only possible to find the exact value of R_1 for a very low frequency, although, for the remaining frequencies are shown the possible values that R_1 and X_1 can assume, which may help guide the analysis of how the circuit operates.